Article type : Original Manuscript

Clinoform development and topset evolution in a mud-rich delta – the Middle Triassic Kobbe Formation, Norwegian Barents Sea

Tore Grane Klausen[a]*, Jonas Aas Torland[b], Christian Haug Eide[a], Behzad Alaei[b], Snorre Olaussen[c], Domenico Chiarella[d]

[a]Department of Earth Science, University of Bergen, Allégaten 41, 5007, Bergen, Norway

[b]Point Resources, Grundingen 3, 0250 Oslo, Norway

[c]The University Centre in Svalbard, Longyearbyen, Norway

[d]Department of Earth Sciences, Royal Holloway University of London, Egham, Surrey TW20 0EX, UK

*Corresponding author: tore.klausen@uib.no

Associate Editor – Piret Plink-Björklund

Short Title – Clinoform and topset evolution of a mud-rich delta

Keywords – Anisian, Barents Sea, clinoform, mudstone-dominated deltas, topset evolution

ABSTRACT

Clinoform surfaces are routinely used to mark transitions from shallow waters to deep basins. This concept represents a valuable tool for screening potential reservoir intervals in frontier basins where limited data are available. Variations in the character of clinoform geometries and shoreline and shelf-edge trajectories are indicators of a range of different factors, such as

palaeobathymetry, changes in relative sea-level and sediment supply. Applications of conceptual and generalized models might however lead to erroneous assumptions about the supply of coarse-grained material to the delta front and basin when superficial similarities between clinoform geometries are not treated holistically. The present study examines the mudstone-dominated Middle Triassic Kobbe Formation – a potential hydrocarbon reservoir interval in the Barents Sea, where prodeltaic to deltaic deposits can be examined in cores, well logs and two-dimensional and three-dimensional seismic data. Despite pronounced acoustic impedance contrast to the surrounding shale, channel belt networks are not observed close to the platform-edge in seismic datasets, even at maximum regressive stages. However, sub-seismic prodeltaic deposits observed on the shallow platform indicate that prodeltaic deposits were sourced directly from the delta plain. Clinoform surfaces with different geometries and scale are observed basinward of the palaeo platform-edge of underlying progradational sequences, correlative to mudstone-dominated prodeltaic core sections. Results indicate that platform-edge deltas developed at discrete sites in the basin due to normal regression, but the positions of these deltas are not directly relatable to variations in clinoform geometries. Transitions from third-order to fourth-order clinoform geometries record discrete transgressive–regressive cycles but are not necessarily good indicators of sandstone deposition. Because of prolonged periods with high accommodation, channel avulsions were frequent and only very fine-grained sandstone was deposited in heterolithic units at the delta front. Sandstones with good reservoir properties are predominantly found along basin margins.

INTRODUCTION

Mudstone-dominated deltaic systems constitute a significant part of the sedimentary record because they are the product of long-lived, large-scale river systems (Orton & Reading, 1993; Syvitski & Saito, 2007; Patruno et al., 2015a; Hartley et al., 2017). Because sandstone accumulations within these depositional systems often are of limited size, highly compartmentalized, of heterolithic nature and scattered over wide areas (e.g. Frazier, 1967; Burpee et al., 2015), such depositional systems are rarely the preferred target for hydrocarbon exploration. Consequently, they remain relatively understudied compared to their more sandstone-rich counterparts. Central issues regarding the development of mudstone-dominated deltaic systems include the process by which sediment is transported to the slope

and basin (Nemec, 1995; Walsh & Nittrouer, 2009; Patruno et al., 2015b; Poyatos-Moré et al., 2016; Gong et al., 2016) and to what extent fluctuations in relative sea-level or sediment supply is driving clinoform progradation (Blum & Törnqvist, 2000; Carvajal et al., 2009; Anell et al., 2014).

The present study uses the Anisian Kobbe Formation to improve the current understanding of ancient large-scale mudstone dominated deltaic successions. This is an ideal case-study of an ancient mudstone-dominated delta system because there are a number of different datasets available which cover the succession on different scales: regional two-dimensional seismic and well logs; local, field scale three-dimensional seismic; and detailed reservoir scale core sections. Importantly, the depositional system is aerially extensive (more than 300 km^2) and the basinward extent of the formation can be constrained within the study area. Moreover, the formation is also interesting because of the difference in reservoir properties between the southern margin and the basin interior. Due to prolific hydrocarbon discoveries in the Goliat Field, along the southern margin of the basin (for example, well 7122/7-3 in Fig. 1), the formation has received considerable interest as a potential reservoir interval. Clinoform topset and channel belts are natural candidates for such reservoir targets, but recent drilling campaigns targeting these deposits have so far been unsuccessful in locating sandstone with good reservoir quality.

To date, studies of the Kobbe Formation have mainly focused on 2D seismic. Notable exceptions are the shallow core descriptions of Mørk & Elvebakk (1999) and Bugge et al. (2002), but these are not fully integrated with seismic data. Thus seismic facies and primarily clinoform geometries interpreted on 2D seismic data are generally used to infer different depositional environments and variations between and within these (Rasmussen et al., 1993; van Veen et al., 1993; Skjold et al., 1998; Riis et al., 2008; Glørstad-Clark et al., 2010; Glørstad-Clark et al., 2011; Lundschien et al., 2014). Following interpretations of steeply dipping oblique clinoform geometries, sea-level has been interpreted to fluctuate during deposition and this has naturally been thought to result in periodic bypass of coarse-grained material to and via what has been interpreted as discrete shelf-edge deltas, or platform-margin deltas, and the basin floor (Rasmussen et al., 1993; Glørstad-Clark et al., 2011; Anell et al., 2014). In more regional studies, sandstone distribution superficially seems extensive since there is no clear definition of which deposits the shallow or marginal marine environment comprise – a depositional environment which is often mapped as continuous belts throughout

the basin in palaeogeographic representations (e.g. Worsley, 2008; Riis et al., 2008; Glørstad-Clark et al., 2010; Lundschien et al., 2014).

In the overlying Snadd Formation, extensive topset deposits have been mapped in a similar mud-dominated progradational system (Klausen et al., 2015). This prograding delta system is characterized by narrow and frequent tidally influenced distributary channel systems, comprised of argillaceous and mineralogically immature fine-grained sandstone, feeding relatively heterolithic delta topsets, with proximal fluvial sandstone deposits showing medium grain size and more favourable reservoir properties (Henriksen et al., 2011; Klausen et al., 2014; Line, 2015). Because the two formations are supplied from the same drainage areas and deposited under equal hydrodynamic conditions in the same basin setting, a similar development should be expected for the Kobbe Formation. Similar deposits have been recognized, but zones of elevated porosity and permeability values have not yet been encountered in the Kobbe Formation. The best reservoir properties are instead found along the southern margin of the basin (i.e. the Goliat Field) and are attributed to a more mature provenance area in the Norwegian Caledonides to the south (Bergan & Knarud, 1993; Mørk, 1999; Ryseth, 2014; Fleming et al., 2016; Eide et al., in press). How far the southerly derived sedimentary systems extend into the basin and how the depositional system has evolved in response to variations in autogenic and allogenic forcing factors is not known, but the reservoir properties of the Kobbe Formation are likely to be governed by the influx and extent of mature sediment from the south in combination with reservoir preserving factors in more central parts of the basin which counter the effects of burial which varied across the basin (Baig et al., 2016).

In order to understand the clinoform progradation and to differentiate between the relative impact and extent of factors controlling reservoir properties within this mudstone-dominated deltaic succession, the present study aims to define depositional elements and environments in the Kobbe Formation based on available core, well and seismic data. This enables a discussion of how these deposits developed through time and how prodeltaic clinoforms are affected by potential autogenic and allogenic variations in their associated deltaic topset and its implications for hydrocarbon exploration in mudstone-rich deltaic systems.

GEOLOGICAL SETTING

The up to 825 m thick Kobbe Formation was deposited after a regional transgression that ended the progradation of the underlying Klappmyss Formation (Dalland et al., 1988; Glørstad-Clark et al., 2011). Depositional environments recorded in the Kobbe Formation range from offshore marine deposits, followed conformably by silt to very fine-grained sandstone, showing an upward shallowing trend into deltaic deposits as the delta prograded (Mørk et al., 1999). Sediments were sourced primarily from an immature provenance region in the south-east Uralides, but also received minor input from more mature provenance areas in the Scandinavian Caledonides to the south (Bergan & Knarud, 1993; Mørk, 1999; Bue & Andresen, 2013). The westernmost parts of the basin might have received sediments from the Upper Palaeozoic to lower Triassic basement as well (Lundschien et al., 2014) but there are no indications of this system prograding into the study area. Organic rich sediments starved of terrigenous influx characterize the distal time-equivalent Steinkobbe Formation found in the western part of the study area (Skjold et al., 1998; Mørk & Elvebakk, 1999). The Anisian to Early Ladinan Kobbe Formation has been defined as a second-order sequence by Glørstad-Clark et al. (2010), subsequently subdivided into four third-order sequences (A1 to A4) defined by discrete maximum flooding surfaces (MFS) [cf. Glørstad-Clark et al. (2011), refining the subdivision of van Veen et al. (1993)].

Post-depositional tectonic history includes Late Jurassic to Cretaceous rifting in the south-western Bjørnøya and Hammerfest basins and Late Cretaceous to Palaeogene uplift and Neogene glacial erosion to the north and west (Gabrielsen et al., 1990; Faleide et al., 1993; Henriksen et al., 2011a). Middle Jurassic normal faulting created the most significant offset within the formation, mainly along the western margin (Bjørnøya Basin) but also in the Hammerfest and Nordkapp basins and on the Bjarmeland Platform (Swaen Graben) (Gabrielsen et al., 1990). Subsequently, Eocene tectonic events firstly compressed and sheared the western margin of the Barents Sea before rifting between Greenland and Svalbard developed into the present Norwegian Sea (Faleide et al., 1993, Worsley et al., 2008). Consequently, the western margin of the Norwegian Barents Sea is presently downfaulted and covered by thick successions of Cenozoic sediments (Faleide et al., 1996). The Kobbe Formation is for the most part preserved throughout the study area, except for above local salt domes in the Nordkapp Basin and above the Svalis Dome. Net exhumation varies from down to *ca* 800 m in the Hammerfest Basin, up to *ca* 2400 m on the Bjarmeland Platform (Baig et al., 2016).

DATA AND METHODS

This study uses a combination of well logs, core and 2D and 3D seismic data to describe the depositional system in the formation (Fig. 1). Data coverage is better in the south-western part of the Norwegian Barents Sea because this area is open to hydrocarbon exploration. Core data presented here includes the longest cores obtained from the Triassic succession in the Barents Sea to date, along with more sparse and scattered core intervals and shallow stratigraphic cores. Attribute maps from 3D seismic facilitate comparison between lithologies in wells with plan-view architecture of sediment bodies within the Kobbe Formation. Wells used in the present study are spaced between 35 km and 125 km apart (Fig. 1) and from these wells, eight core intervals have been studied, ranging from a few metres (7324/10-1) up to *ca* 164 m (7222/11-2). Regional 2D seismic profiles are spaced about 2 km apart and are used for regional extrapolation of sequence boundaries and facies.

Eight 3D seismic surveys are used in this study (Fig. 1), all of which has been pre-stack time migrated with inline and cross line spacing in the range of 12.5 to 25.0 m. The data is noise cancelled and both full and far angle stacks of the surveys have been used. For the purposes of this study, far-angle stack data resulted in the better imaging of the depositional elements within the formation and, with the exception of Survey H (Fig. 1) which was adequately imaged in full stack data, the 3D seismic presented below are far-angle stacks. Higher incident angles do in some cases amplify the amplitude of a seismic event (Ostrander 1984; Castagna 1993; Carter 2003), but a detailed account of these AVO effects on lithology are beyond the scope of the present paper. The dominant frequency of the seismic data in the Kobbe Formation depth varies from 25 to 38 Hz (Fig. 2A). All of the 3D data used in this study has a 4 ms sampling rate. Vertical seismic resolution (which is the minimum measureable thickness between top and base of a layer) within the 3D data is estimated using the frequency information derived from spectral decomposition, and the interval velocity data derived from the well velocity surveys in and around the 3D surveys (Fig 2B). Vertical resolution is achieved by dividing the dominant wavelength at target interval by four which gives thickness ranges from 14 to 33 m. However, the limit of visibility for a given layer (Widess, 1973) is one eighth of the dominant wavelength, in this case *ca* 7 to 17 m. Increased resolution might be achieved with high-frequency P-Cable seismic data in intervals at shallow depth. Since the data are migrated, lateral resolution of the surveys is generally high and varies between 15 m and 45 m.

Amplitude derived from full bandwidth seismic data may not adequately image all geological features and therefore spectral decomposition has been utilized in order to extract amplitude information from certain frequency ranges. Spectral decomposition creates a continuous time-frequency analysis of seismic data (e.g. Castagna & Sun, 2006) that can be utilized to convert broad band seismic data into discrete frequency or frequencies. This study employed spectral decomposition using a wavelet transform based approach (e.g. Castagna & Sun, 2006) and matched-pursuit decomposition technique (Castagna et al. 2003; Liu and Marfurt 2007) to decompose the seismic volumes into magnitudes of different frequencies. Resulting frequency volumes are blended using red, green and blue colour ranges. Selection of the different frequencies depends on the seismic amplitude response of every individual frequency volume at the target interval. Target intervals were defined by iso-proportional slicing of individual sequences.

TERMINOLOGY

Figure 3A illustrates how the different segments of the clinoform surface are used in the present study and the difference between sigmoidal (S) clinoform surfaces, characterized by topset accommodation, and oblique (O) clinoform surfaces, characterized by limited topset accommodation (Mitchum et al., 1977; Sangree & Widmier, 1977; Pirmez et al., 1998; Catuneanu et al., 2009). Intermediate shapes between these end-members are referred to as complex sigmoidal (cf. Mitchum et al., 1977). Clinoform segment definitions are adapted from Patruno et al. (2015a).

Clinoform geometries are developed in a range of different depositional environments and form at different scales (Helland-Hansen et al., 2012; Fig. 3B). Because of the wide range of scales at which they appear, the topset of subaqueous clinoforms are interchangeably termed platform and shelf in the literature (e.g. Galloway, 1975; Sydow & Roberts, 1994; Steel et al., 2003; Porębski & Steel, 2003; Carvajal et al., 2009; Glørstad-Clark et al., 2010; Helland-Hansen et al., 2012; Sylvester et al., 2012; Dixon et al., 2012; Laugier & Plink-Björklund, 2016; Gong et al., 2016; Poyatos-Moré et al., 2016). The present study reserves the term shelf as the definition of the topset of continental margin scale clinoforms (*ca* 500 m to thousands of metres) and platform as the definition of the topset of shelf prism clinoforms which are formed on the shelf, whereas for the topset of subaqueous delta clinoforms the term subaqueous delta top is preferred (cf. Patruno et al., 2015a). While the term shelf prism gives

an appropriate sense of scale for the Kobbe Formation compared with other basins, it can be confusing in this case because the contemporaneous shelf-edge proper is not seen in direct connection with the clinoforms in the basin. The contemporaneous continental scale clinoforms might have been forming detached from these clinoforms in areas to the north, outside of the study area, or alternatively: the apparent detachment could simply be due to the Kobbe Formation clinoforms having developed in a relatively shallow basin without an associated continental margin. Therefore, the term platform is used instead of shelf prism herein (cf. Glørstad-Clark et al., 2011). Shelf edge deltas develop where the subaerial delta progrades across the underlying shelf edge, at which point it might distribute sediments directly to the basin floor (Porębski & Steel, 2003; Carvajal & Steel, 2006). Because the Kobbe Formation is characterized by platform clinoforms, the term platform edge delta (cf. Anell et al., 2014) is used herein for deltaic progradation basinward of the platform edge (Fig. 3C).

As is common in many other depositional systems, the Kobbe Formation comprises clinoform geometries of different scale (Fig. 4). These can be categorized based on the stratigraphic hierarchy in which they are developed, and are described here based on their relation to the sequence stratigraphic framework provided in Glørstad-Clark et al. (2011): (i) Second-order clinoform surfaces corresponds to and formed above the MFS that bounds second-order sequences within the basin. The Kobbe Formation itself represents a second-order sequence, and its upper and lower boundaries are sigmoidal second-order clinoforms. (ii) Third-order clinoforms are formed by the same processes of periodic landward displacement of the shoreline and also results in sigmoidal geometries. These surfaces follow above third-order MFS and are probably formed over shorter periods of time, with less condensation compared to its second-order equivalents. This is reflected in less well-defined seismic reflection signals compared to the second-order clinoform surfaces which corresponds to organic-rich, high gamma ray, well-log motifs (Fig. 4). (iii) Fourth-order clinoform surfaces occur as oblique or complex sigmoidal basinward dipping reflectors (*sensu* Mitchum et al., 1977; Glørstad-Clark et al., 2010) in the upper part of each third-order sequence (Fig. 4). These clinoform surfaces downlap onto the third-order clinoform surfaces below.

FACIES ANALYSIS

Different depositional environments have been categorized earlier based on: basinward-dipping seismic reflectors of different character (prodelta); parallel continuous reflectors (shelf); and chaotic and discontinuous reflectors (shallow and non-marine) (Fig. 4). Core data from the upper A4 sequence add more detail to this understanding and can be used to describe seismic facies based on their appearance in core and well logs. Characteristic expressions in seismic attribute maps are also discussed. Facies associations encountered in the formation are summarized in Table 1.

Offshore (Facies Association 1)

The most distal deposits of the formation have not been studied in core directly, but an equivalent of this facies association (FA1) is recorded in the Snadd Formation just above the study interval investigated here (Fig. 5B). It consists primarily of non-stratified grey siltstone with thin, discontinuous laminae of fine-grained sandstone. The well log character is however characteristic in relation to its high gamma ray values, in addition to high neutron porosity and low density.

Interpretation: High gamma ray and neutron porosity readings suggest organic-rich, sediment-starved, condensed sections and although FA1 is only studied in core from a relatively proximal position with grey siltstone and very fine sandstone laminae, previous studies document condensed, organic-rich deposits which span the Olenekian, Anisian and Ladinian and correspond to the Steinkobbe and Botneheia formations in the western part of the study area (Mørk & Elvebakk, 1999; Mørk et al., 1999). The facies association is followed stratigraphically by more proximal deposits (FA2). Accordingly, FA1 is interpreted to have been deposited in an offshore marine environment. This is corroborated by seismic data, discussed below.

Prodelta (Facies Association 2)

Facies Association 2 (FA2) is characterized by structureless to laminated grey siltstone which is commonly bioturbated by *Planolites* and interbedded with thin (2 to 10 cm) beds and discontinuous lenses of very fine sandstone, some of which grade normally into siltstone and others also show slightly sinuous lamination (Fig. 6G). These deposits comprise an up to *ca* 150 m thick succession overlain by coarser grained deposits in the core from 7222/11-2 (Fig. 6). In the lower middle part of this succession, two discrete units of relatively thicker (10 to

50 cm) very fine-grained sandstone beds are planar to cross-laminated and show sharp erosional bases and tops. Locally, normal to inverse grading to siltstone are stacked in up to 8.5 m thick units (for example, Fig. 6I). The upper middle part of the succession comprises a single bed with soft sediment deformed original lamination followed by massive, structureless grey siltstone with fluid escape structures (Fig. 6F). This facies association is characterized in well logs by thick (100 to 200 m) predominantly high, but serrated, gamma ray trends with occasional blocky to upward decreasing and increasing gamma ray lows of about 5 m (Figs 4 and 6).

Interpretation: Thin beds of normally graded very fine sandstone are interpreted as slope apron turbidite deposits (cf. Stow et al., 1983), whereas more lens-shaped, irregular and sinuous sandstone deposits which show signs of currents reworking with fluctuating energy are interpreted to be deposited by contour currents (cf. Shanmugam, 2012; Rebesco et al., 2014). These characteristics are also typically found in turbidite deposits, but the contourite deposits interpreted here are distinguished by mud-laminae on foresets (for example, Fig 6G). Relatively larger scale beds of very fine sandstone in the lower middle part of the succession are variable both in terms of thickness and contacts. Although most beds are sharp-based and grade into shale representing the classical Bouma sequences, some show inverse grading indicating waxing hydrodynamic regime (Fig. 6I). Because of the repeated, but irregular pattern of waxing and waning flow, these turbidite beds are interpreted to be deposited by hyperpycnal flows (cf. Plink-Björklund et al., 2001; Mulder & Syvitski, 2003; Bhattacharya & MacEachern, 2009; Lamb & Mohrig, 2009). The soft-sediment deformation is interpreted to be caused by slumping in the upper middle part of the prodelta slope and indicate slope instability. Alternatively, deformation is caused by fluid escape, also caused by increased sedimentation rates but without slope instability. In addition to the depositional processes mentioned above, homogenous siltstone (for example, Fig. 6F and G) might have been deposited by flocculated silt and mud (cf. Schieber & Southard, 2009). The well log character reflects the dominance of siltstone and sporadic occurrences of sandstone with variable thicknesses. Therefore, FA2 is interpreted as prodeltaic.

Shallow marine (Facies Association 3)

Facies Association 3 (FA3) is found stratigraphically above the prodelta deposits (FA2) and is characterized by very fine to fine-grained sandstone associated with a range of sedimentological structures: (i) wavy to flaser bedded sandstone (30 cm to 4 m thick) with

mud drapes, non-stratified mud deposits and reactivation surfaces interbedded with siltstone. Bioturbation is sparse, mostly *Planolites* (Fig. 7F); (ii) up to 2.4 m thick sandstone with chaotic and irregular lamination, highlighted by carbonaceous material along bedding planes, in addition to unidirectional cross lamination (Fig. 6E) with no bioturbation; (iii) 1 to 4 m thick sandstone with plane parallel lamination, bidirectional cross-lamination and shell fragments with relatively diverse and intense bioturbation (Fig. 5E), including *Planolites, Teichicnus, Skolithos* and *Diplocraterion*. Sandstones interbedded with silt naturally show a more erratic gamma ray signal compared to the generally low gamma ray signal which characterize the facies association (Fig. 6A).

Interpretation: Wavy to flaser bedded sandstone interbedded and interlaminated with siltstone along with non-stratified mudstone which indicate fluid mud deposition are interpreted to represent tidal sandflat deposits (Flemming, 2012), whereas slightly coarser sandstone with plant fragments and chaotic lamination indicate more rapid and episodic deposition, such as in a mouth-bar setting (cf. Coleman et al., 1964; Roberts et al., 1980). Relatively more diverse bioturbation in planar laminated sandstone is interpreted to be deposited in a shoreface setting or as transgressive lags (Clifton, 2006). These three distinct facies are collectively referred to as shallow marine environment (FA3).

Coastal plain (Facies Association 4)

Facies Association 4 (FA4) occurs stratigraphically above the shallow marine (FA3), is characterized by siltstone, mud, siltstone, very fine-grained sandstone and coal, and ranges in thickness from a few centimetres to 6 m (Fig. 8). The siltstone is either: rooted and gradational to coal; mottled with clay aggregates of greenish-white to reddish colour; or grey interbedded with sandstone with intense to moderate bioturbation (Fig. 6D). The well log signal is characterized by: (i) low to moderate gamma ray values, which might be serrated; and (ii) high neutron log values for the coal deposits while the density log is characteristically low.

Interpretation: This facies association is characterized by three distinct facies reflecting varying amounts of marine influence and wetting and drying which can be related back to shoreline proximity. In particular, coal and carbonaceous shale are interpreted as the water-logged parts of the floodplain with little marine influence and limited sediment influx (Diessel, 2006); the multicoloured, mottled siltstones are interpreted as vertisols and reflect periodic wetting and drying of the floodplain (Mack et al., 1993); grey siltstone with marine

influence is interpreted to have been deposited in interfluvial bay areas (cf. Coleman et al., 1964). These facies are collectively referred to as coastal plain (FA4).

Channelized deposits (Facies Association 5)

Facies Association 5 (FA5) is encountered stratigraphically above shallow marine deposits (FA3) and both above and below coastal plain deposits (FA4). It is characterized by fine to medium-grained sandstone with two distinctly different characteristics. (i) A generally grey coloured, argillaceous fine-grained sandstone up to 19 m thick characterized by discrete intervals of abundant intraformational rip-up mud clasts, mud drapes and non-stratified mud deposits (Fig. 5C). Discrete beds range in thickness from *ca* 0.5 to 1.5 m. Sparse *Planolites* bioturbation is observed. (ii) The other sandstone deposits within FA5 are up to 10 m thick, fine to medium-grained and show unidirectional cross-stratification or chaotic lamination. Fine-grained material and abundant plant fragments highlight laminae. Both facies have erosive bases and blocky to slightly upward increasing gamma ray values. The former facies has spikes of high gamma ray values in horizons characterized by abundant rip-up mud clasts.

Interpretation: Fine-grained argillaceous sandstone with frequent mud drapes, fluid mud deposits and sparse bioturbation are interpreted as tidally influenced distributary channel deposits (cf. Martinius & Van den Berg, 2011). Horizons with rip-up mud clasts are interpreted to represent discrete episodes of cut bank erosion and downstream deposition at channel bends. Despite a number of discrete beds recording phases of cut-bank erosion, there are no indications that the channel deposits are amalgamated and multi-storey. Facies with more homogenous sandstone, unidirectional cross-lamination and chaotic lamination with plant fragments are interpreted as fluvial channel deposits (Bridge, 2006). The latter is encountered in core closer to the basin margin (Fig. 7C), where it is associated with coastal plain deposits with limited marine influence, but is transitional to the tidally influenced channel deposits in the basin. Similar to the tidally influenced channels, the fluvial dominated ones are also single-storey. The facies are collectively referred to as channelized deposits (FA5).

Characteristics of facies associations in two-dimensional seismic

Well logs tied to seismic show that the 2D seismic expression of offshore deposits (FA1) is characterized by high-amplitude parallel reflectors which are often planar and followed stratigraphically by downlapping, basinward dipping seismic reflectors of the prodelta (FA2; Fig. 9). Facies Association 2 is represented both by flat, parallel reflectors in shallow platform areas above the delta-plain of the previous sequence, and inclined seismic reflectors characteristic of clinoform surfaces basinward of the platform-edge of underlying sequences. Core from well 7222/11-2 shows a 150 m upward coarsening sequence from prodeltaic turbidites to deltaic deposits (Fig. 6) which correspond to an upward shallowing well log trend in the platform area of the A4 sequence but is not associated with any type of clinoform surface (Fig. 9). The well log trend of the prodeltaic core interval is however identical to wells that penetrate the clinoform succession (Fig. 8F), and since third-order and fourth-order clinoform surfaces are seen directly basinward of the normal regressive core section (Fig. 9) the deposits comprised within the different clinoform successions are interpreted to be equal to those of the prodelta in core from 7222/11-2 and its distal equivalents.

Shallow marine (FA3) and coastal plain (FA4) deposits are generally characterized by heterogeneous to transparent seismic reflectors in 2D seismic, and both facies are weakly parallel and chaotic. These facies associations are found stratigraphically above parallel reflectors of the prodelta (FA2), and commonly encase discontinuous, high amplitude reflectors of channelized deposits (FA5, Fig. 9). Similar characteristics have been used to distinguish between seismic facies in previous studies (e.g. Riis et al., 2008). Shallow marine (FA3) and coastal plain (FA4) deposits are interconnected and transitional to one another, and core sections show that the latter contain coal deposits and palaeosol horizons in eastern and southern parts of the study area (for example, Figs 5, 7 and 8), which indicates more continental environments and periodic subaerial exposure in these more proximal parts of the basin. Channelized deposits (FA5) are characterized by discontinuous high amplitude reflectors in 2D seismic cross-sections. The typical seismic event is about 20 m thick, indicating a tuning thickness effect around the lower thresholds of seismic resolution (Brown, 2004), and the width of the discontinuous amplitude that characterize the facies association varies according to how the seismic profile is oriented relative to the facies association. In core, channelized deposits (FA5) vary between tidally influenced distributaries and fluvial channels (see Figs 6 and 7), but only the former have yet been confidently tied to seismic reflectors because their fluvial counterparts have so far not been cored within the formation.

Facies characteristics in three-dimensional seismic

Depositional elements are only observed in attribute maps in the uppermost part of each sequence. These parts are generally characterized by low-sinuosity seismic reflectors that trend towards the north-west (Fig. 10). The discontinuous high amplitude events are up to 5 km wide in plan view in the south-eastern part of the study area (Fig. 9D), where they are observed to have developed into sinusoidal or discrete convex sets of high-amplitude reflectors. Similar seismic geomorphologies are at most *ca* 1.5 km wide in the western part of the study area (Fig. 10B). In contrast to the upper sequences, the lowermost part of the succession only shows seismically resolvable channelized deposits in the south-east.

The seismic reflectors which are highly sinuous to elongate in plan view correspond directly to low gamma ray readings in wells that penetrate them, and core material from these wells is characterized by fine-grained sandstone with rip-up mud clasts and fluid mud interpreted as tidally influenced channel deposits (FA5). The sinuous reflectors are therefore interpreted to represent tidally influenced distributary channel and channel belt deposits in a heterolithic coastal plain environment (FA4). Fluvial channel deposits could not be directly tied to core intervals, but proximal equivalents to the tidally influenced channel deposits are expected to be increasingly more fluvial dominated (for example, Fig. 10C), as is also seen in the coastal plain facies from core (see Figs 5F, 7B and 8E). Lack of seismically resolvable deposits in the lowermost sequence is most likely to be related to proximal–distal trends in the channelized deposits. Distal thinning into terminal distributaries (Olariu & Bhattacharya, 2006) could result in deposits below seismic resolution. In the main distributary channels however, channel deepening resulting from drawdown effects as the river plume adjust to sea-level in the backwater zone of the delta during river floods (Lamb et al., 2012) probably result in thickening of the channel deposits distally. Additionally, the tidal signatures in the channelized deposits of the Kobbe Formation (for example, Fig. 6B) suggest that the channels might have been prone to deepening related to tidal currents, in accordance with results from modelling tidal influence on channels (Rossi et al., 2016). Channelized deposits in distal parts of the overlying Snadd Formation are indeed characterized by increasing thicknesses basinward (Klausen et al., 2014). The absence of channelized deposits in distal parts of the sequences in the Kobbe Formation could alternatively be related to lower acoustic impedance contrast between channelized deposits and encasing shallow marine facies associations (FA3), which is reconcilable with the proximal–distal increase in marine influence and deposition of finer grained material.

STRATIGRAPHIC ARCHITECTURE

Details from core in the A4 sequence demonstrate how the depositional system evolved in the later stages of the formation. By comparing geometries, seismic facies and well logs from this interval with underlying sequences, the regional and temporal development of the formation can be assessed. Regional correlation of well logs (Fig. 11) shows how the discrete packages of upward shallowing facies associations presented above relate to the sequence stratigraphic framework presented by Glørstad-Clark et al. (2011).

A4 sequence

This sequence is defined as the youngest of four pronounced upward shallowing successions in the formation (Glørstad-Clark et al., 2011; Paterson & Mangerud, 2017; Fig. 11). It corresponds to the palynozones *Protodiploxypinus decus* and *Triadispora obscura* of Vigran et al. (2014) in well 7324/10-1, which are independently dated as Late and Middle Anisian based on ammonoids. The sequence is up to 270 m thick within the study area and is dominated by prodeltaic (FA2), overlain by shallow marine (FA3), channelized deposits (FA5) and coastal plain (FA4) in the more proximal parts of the study area. At its base, the sequence has an unconformable transition to the underlying deltaic topset of the A3 sequence characterized by a regional MFS. This flooding is followed by an upward shallowing sequence of predominantly offshore marine, prodeltaic shale deposits in core from 7222/11-2 (Fig. 6). Prodeltaic deposits are followed stratigraphically by channelized deposits (FA5) which are seen in 3D seismic as pronounced channel belts (Fig. 10). These deposits are more well-developed and found further basinward in the A4 sequence than in the previous sequences. Seismic cross-sections are characterized by parallel seismic reflectors overlying the A3 sequence, and prodeltaic clinoform surfaces (FA2) basinward to the platform-edge of the maximum regressive stage of the A3 sequence. Clinoform surfaces in the A4 sequence are best developed in the areas around the Hoop Fault Complex (Figs 1 and 12).

A3 sequence

This sequence is defined as the third pronounced upward shallowing succession in the formation (Glørstad-Clark et al., 2011; Fig. 11). It corresponds to the upper part of palynozone *Anapiculatisporites spiniger* of Vigran et al. (2014) in well 7324/10-1, which is independently dated as Early Anisian based on ammonoids (Weitschat & Dagys, 1989). The sequence is up to 230 m thick within the study area and is dominated by prodeltaic (FA2),

shallow marine (FA3) and channelized deposits (FA5). The base corresponds to an abrupt flooding of the topset of the A2 sequence. There is no core material available from this sequence, but 3D seismic data reveals channel belt deposits on the Bjarmeland and Finnmark platforms (Fig. 13A and B). The channel deposits are generally narrower than the channel belts described in the overlying sequence. Seismic cross-sections are characterized by parallel seismic reflectors overlying the A2 sequence, and prodeltaic clinoform surfaces (FA2) are best developed in the areas around the Loppa High (Fig. 13C).

A2 sequence

This sequence is defined as the second pronounced upward shallowing trend in the formation (Glørstad-Clark et al., 2011; Fig. 11). It corresponds to the middle part of palynozone *Anapiculatisporites spiniger* of Vigran et al. (2014) in well 7324/10-1. The sequence is up to 220 m thick within the study area and is dominated by prodeltaic deposits (FA2), overlain by shallow marine (FA3) and channelized deposits (FA5). There is no core material available from this sequence, but 3D seismic data reveals channel belts on the Bjarmeland Platform (Fig. 14A) and in the eastern part of the basin (Fig. 14B). Seismic cross-sections are generally characterized by parallel seismic reflectors overlying the A1 sequence, but show stratal terminations of fourth-order clinoform surfaces downlapping onto third-order surfaces in the west (Fig. 14C). Clinoform surfaces (FA2) are most pronounced in the areas around the Loppa High (Fig. 1), where they correspond directly to the thickest parts of the sequence.

A1 sequence

This sequence is defined by the first upward shallowing trend in the formation (Glørstad-Clark et al., 2011; Fig 11). It corresponds to the lower part of palynozone *Jerseyiaspora punctispinosa* of Vigran et al. (2014) in well 7324/10-1, and is up to *ca* 200 m thick within the study area. There is no core material available from this sequence, but well logs coupled with seismic indicates that the sequence is dominated by prodeltaic clinoforms (FA2), overlying thin offshore deposits (FA1). Three-dimensional seismic attribute maps reveal some indications of channel belts in the south-eastern part of the study area (Fig. 15B). Seismic cross-sections are characterized by parallel seismic reflectors above the Klappmyss Formation MFS in the most proximal parts of the basin, but generally show downlapping stratal terminations of fourth-order (intra-A1) clinoform surfaces on this MFS over a larger area than is the case for overlying sequences (for example, Fig. 15A). Clinoform rollovers indicate a flat platform-edge trajectory and topsets generally show parallel reflectors.

Prodeltaic clinoform surfaces (FA2) are best developed in the areas around the Hoop Fault complex (Figs 1 and 15A), far separated (*ca* 150 km) from the only channel deposits observed in 3D seismic on the Finnmark Platform (Figs 1 and 15B).

Thickness variations

Thickness variations in the Kobbe Formation are directly related to the accommodation available in front of the underlying Klappmyss Formation platform-edge and subsequent sequences (Fig. 16). Each sequence is constrained in a western basinward direction by relatively abrupt terminations. It is evident from the thickness map of each discrete third-order sequence that the Kobbe Formation sequences are characterized by extensive topset accumulation landward. Individual sequences gradually filled the basin with approximately equal progradational distance (Fig. 17) and thickness (10 to 25 km basinward and up to 100 to 200 m thick). However, sediments seem to be unevenly distributed across the study area at any given time. Although progradation distance is greatest in the area east of the Loppa High (Fig. 17), the main depocentres in terms of accumulated thickness shift from the southern Bjarmeland Platform in the lower A1 and A2 sequences (Fig. 16A and B), and move progressively northward toward the Maud Basin in the upper A4 sequence (Fig. 16D).

Thickness trends seem to reflect the gradual infill of available accommodation in front of previous sequences. The most distal 3D seismic datasets (Survey A and B, Fig. 1) have the lowest dominant frequencies of the surveys within the Kobbe Formation (Fig. 2A), and hence the lowest resolution, the distal surveys show no indications of channelized deposits. This is substantiated by well logs from corresponding positions (Fig. 8F). Given that distributary channel networks are resolved in 3D seismic, the orientation of imaged channels does not reflect any preferential orientation towards areas of increased thickness (Fig. 17) and it is unlikely that these areas represented more pronounced topographic lows at the time of deposition. It also seems that the A1 sequence is thinner relative to other sequences and that its area of increased thickness is more widespread than the following sequences. This is reflected by the more widespread occurrences of fourth-order clinoform surfaces (for example, Fig. 15A).

In the three oldest sequences (A1 to A3), the thickest part of each sequence is related to the prodeltaic clinoform succession (for example, Figs 13A, 14C, 15A and 15B). Conversely, in the youngest A4 sequence relatively thick parts formed east of the Loppa High and in the Hoop Fault complex (Fig. 15D) at a later stage of the A4 sequence and are not directly related

to clinoform development as seen in Figs 12D, 13C and 14C. This local thickening attests to some degree of syn-depositional compaction and subsidence in the topset of the A4 sequence, and in the Hoop Fault Complex Area it directly affects clinoform geometries and the platform-edge trajectory of underlying deposits (Fig. 12D). The thickness increase might also have been subsequently affected by differential subsidence and compaction around the basement high underneath the Loppa High (Wood et al., 1989) and above the Hoop Fault complex (Gabrielsen et al., 1990).

The Loppa High (Fig. 1) is suggested to have been elevated at least partially during deposition of the Kobbe Formation (Glørstad-Clark et al., 2011) and this might have affected the thickness trends in the formation. In particular, a northward shift of higher rates of sediment accumulations in the A4 unit might be consistent with such an interpretation because an elevated Loppa High could have forced sediment accumulation in this direction. However, there are no depositional features (for example, clinoform surfaces) which indicate deflection in response to this suggested high. It is also worth noting that the large scale development of the Kobbe Formation shows only minor indications of being affected by the Loppa High: the thickest part of the formation which reflects the accumulated thickness of all clinoform successions shows an overall linear trend, but the area with increased thickness is slightly more widespread above the suggested high (Fig. 18). The A3 and A4 sequences have developed a slight protrusion in the platform-edge above the Loppa High (Fig. 16C and D) which might be related to a platform-edge delta in this area. This interpretation is consistent with observations from 3D seismic, where most of the channelized deposits are observed in surveys from the southern part of the basin, trending towards the Loppa High (Fig. 16).

DELTA AND CLINOFORM PROGRADATION

Combining core material with 2D and 3D seismic explains the depositional processes of the prograding delta. This understanding can be extended to variations in clinoform geometries within the A4 sequence and sequences below. Clinoform surfaces correspond directly to the thickest part of each sequence within the Kobbe Formation; however, from the well tie of 7222/11-2 (Fig. 9) it is evident that up to 150 m thick prodeltaic successions developed on the platform without creating basinward dipping clinoform surfaces. This section evaluates the main controls on the clinoform development in light of the findings presented above (Figs 12

to 16), with implications for understanding the depositional processes in mud-dominated clinoform successions and the relationship between clinoform surface of different scales.

Clinoform development in relation to deltaic topsets

Prodeltaic deposits (FA2) are mainly characterized by heterolithic siltstone and thin turbidite deposits (Fig. 6). Episodic deposition of thin-bedded turbidite beds over wide prodeltaic areas is therefore interpreted to act as the main dispersal mechanism for sediment during delta progradation. Turbidite deposits formed on the gentle prodeltaic slope (Fig. 18) are interpreted to be deposited by hyperpycnal flows (cf. Plink-Björklund et al., 2001; Mulder & Syvitski, 2003; Plink-Björklund & Steel, 2004; Bhattacharya & MacEachern, 2009; Lamb et al., 2010) sourced directly from the distributary channels during delta progradation. This is primarily based on sedimentary structures which indicate alternating waxing and waning flow regimes in a series of turbidite beds (Fig. 6I) and is supported by the fact that such deposits are found stratigraphically below mouth bar and deltaic deposits in a normal regressive upward shallowing sequence (Fig. 6). Alternatively, the subaerial delta could potentially have been detached from the contemporaneous platform edge by a subaqueous delta (Fig. 3), but core intervals from the prodeltaic succession in well 7222/11-2 do not show any distinct storm deposits or pronounced offshore tidal bar deposits that suggest efficient redistribution of sandstone from the subaerial to the subaqueous delta front (Patruno et al., 2015b; Poyatos-Moré et al., 2016). Instead, the upward shallowing succession is dominated by silt, and most of the very fine-grained sandstone is interpreted to be deposited by dilute low density flows (Fig. 6G) and redistributed by longshore currents (Figs 6G and 7F) and occasional slumping (Fig. 6F). This is interpreted to reflect delta progradation attached to its contemporaneous distal bottomset, feeding hyperpycnal turbidite lobes directly from the river mouth without an intermittent subaqueous delta staging area.

In the facies section above, well logs that penetrate discrete clinoform successions were compared to the well log associated with the prodeltaic core interval in 7222/11-2 (Fig. 8F) and these showed distinct similarities. In addition, the core interval from 7222/11-2 records a normal regressive trend from prodelta to shallow marine and deltaic deposits which is substantiated by the fact that seismic-scale channelized deposits are not observed close to the platform-edge delta at any maximum regressive stage (Figs 16 and 17). The most distal 3D seismic surveys (A and B in Fig. 1) in the study area have the lowest resolution (Fig. 2A), but channelized deposits similar in thickness to FA5 in 7222/11-2 (Fig. 6) are still within the

resolution threshold and would be expected close to the platform-edge in a scenario with forced regression and incision (e.g. Posamentier, 2001). Smaller scale channels linking the distributary channel to its terminal mouth bar deposits could exist below seismic resolution in the most distal part of the delta system, but their potential presence is not diagnostic for incision. Considering the normal regressive nature of the prodeltaic succession, combined with the fact that clinoform geometries of the third-order and fourth-order are located directly basinward of the prodeltaic core section (Fig. 9), it is reasonable to interpret the clinoform successions to be composed of the same deposits as seen in core sections from the platform (Fig. 19).

The present core material furthermore suggests that the turbidite deposits are close to or below the lowest possible resolution threshold; this is substantiated by the comparably thin turbidite deposits (up to 6.5 m) documented by Mørk & Elvebakk (1999) from the distal parts of the underlying Klappmyss Formation in the IKU-well (7323/07-U-06 to 7323/07-U-06-08). This explains why no turbidite deposits are observed in seismic from the study area but also illustrates that the present authors cannot draw conclusions based on their presence or absence based on seismic data. Wells off-axis to the distributary channels indicate that there are few obvious candidates for turbidite deposits in these northern and distal areas (for example, 7324/10-1 in Fig. 8F, and 7324/7-1S and 7324/10-1 in Fig. 11). Contour currents are instead interpreted to have facilitated reworking and lateral distribution of sediment (cf. Rebesco et al., 2014), and the prodeltaic deposits recorded in this study thus reflect a mixture of different processes: periodic currents (Fig. 6H) and slumps (Fig. 6F); occasional floods (Fig. 6I); and prevalent contour drift (Fig. 6G).

The coarsest material recorded from the basin centre (fine to medium-grained sandstone) is found in mouth-bar deposits (FA3) of the A4 sequence in 7222/11-2 (Fig. 6E). It has been deposited in the upper part of the conformable upward shallowing succession, more proximal than the A4 shelf-edge delta (Fig. 19). These mouth-bar deposits are interpreted to have been deposited by a flooding event in the distributary channel system, causing influx of sediments which are coarser and more rapidly deposited than the tidally influenced channel deposits (FA5) stratigraphically above (Fig. 6). The more fine-grained channel sandstone is clearly separated from the mouth bar deposits by marine dominated coastal plain deposits (FA4, Fig. 6D) and suggests that a more stable distributary channel system was established after the flooding event which deposited the mouth bar in the initial phase of delta lobe progradation (cf. Slingerland & Smith, 2004). Shallow marine (FA3) deposits in the Kobbe Formation are

however typically more fine-grained, bioturbated and heterolithic than these mouth bar deposits, suggesting a less catastrophic and weaker hydrodynamic regime (for example, Figs 5E and 7B).

Core data from the A4 sequence highlights pronounced proximal–distal trends within the basin. Easternmost parts of the study area (IKU wells 7230/5-U-5 and 7230/5-U-5-6, Figs 5 and 8) and the southern Goliat wells (7122/7-3, Fig.7) contain abundant coal beds from the coastal plain (FA4) and organic fragments in channelized deposits (FA5) in the upper part of the sequence. Presence of coal deposits contrasts with correlative deposits in cored intervals in well 7222/11-2 where the upper part of the sequence is mainly characterized by shallow marine (FA3), exemplified by discrete mouth-bar and tidal deposits (Fig. 6). Lack of well-developed coastal plain (FA4), but relatively thick shallow marine (FA3) and channelized deposits (FA5), suggest that well 7222/11-2 cored more distal deltaic deposits than 7230/5-U-1, 7228/3-U-1 and 7122/7-3 which are located further east and south in the basin. Importantly, core material is not available from the uppermost part of the sequence, but low and stable neutron porosity values combined with homogenous and high-density values in log data (Fig. 6A) suggest the absence of coal horizons. The distal parts of the deltaic topset are found in the central and western parts of the basin and are to a greater extent dominated by marine interaction, and the shallow marine FA3 is the most common in the upper part of the topsets (Fig. 6). This is consistent with higher degrees of tidal influence in the channelized deposits (FA5) found in the distal part of the basin. Coal deposits with roots and palaeosols indicate both subaerial exposure and less stressed environments in proximal, eastern and southern parts of the study area, where coal formed in the periodic absence of marine incursions and recurrent overbank flooding.

Deltaic systems of the Kobbe Formation are interpreted to be normal regressive with increasingly more heterolithic and marine dominated deposits basinward on the delta plain, in front of which discrete successions of clinoform geometries are found in each individual sequence. Clinoform successions are dominated by fine-grained slope-apron turbidite and contourite deposits with no pronounced subaqueous delta staging area in front of the prograding delta, but with sporadic sub-seismic (less than 8.5 m) hyperpycnal flow deposits.

Characteristics of clinoform geometries

The generally fine-grained clinoform successions of the Kobbe Formation comprise distinctly different clinoform geometries which reflect different sequence stratigraphic units, or stages in a series of transgressive–regressive cycles. Clinoform surfaces defining the upper and lower boundaries of each third-order sequence are generally sigmoidal and vary between 150 m and 300 m in height (Figs 12 to 15 and 19) with foreset slope gradients of 1.7°. They are thus of a similar scale as modern and ancient shelf-edge and shelf-prism clinoforms (Patruno et al., 2015a). As indicated by abrupt deepening in well log trends (Fig. 11) compared with stratal terminations of seismic reflectors (Figs 12 to 15), third-order clinoforms are interpreted to form after discrete maximum flooding events at the transition between third-order sequences defined by Glørstad-Clark et al. (2011) when the normal regressive period of the previous sequence is punctuated by significant landward displacement of the delta system (Fig. 19A). These events of increased relative sea-level caused flooding and draping of the underlying third-order sequence and gave rise to the sigmoidal clinoform geometries which scale to platform clinoforms (Fig. 19A). These flooding events are similar to the second-order MFS recorded in core from well 7230/5-U-5 (Fig. 5), and caused lower sedimentation rates on the newly established shallow shelf as a natural consequence of the transgressive event which shifted deposition landward (Fig. 20A). Sedimentation rates are interpreted to have remained restricted until subsequent, gradual progradation of the delta (Fig. 20B and C). Although the actual boundary between the third-order sequences is defined by a distinct MFS event, the clinoform surface associated with this flooding and the clinoforms that conform to this surface are together regarded as third-order clinoform surfaces.

Lack of seismically resolvable clinoforms in the topset above each sequence is interpreted to reflect a very shallow prodelta gradient where several fine-grained slope-apron turbidite deposits (for example, Fig. 6) are deposited progressively basinward over a wide area on a shallow platform with restricted accommodation (cf. Galloway, 1998). Low gradients are likely in a mud-dominated deltaic system (Patruno et al., 2015a). It is likely that some sediment was transported to the platform-edge and beyond during prodeltaic sedimentation on the shallow shelf, with increasing magnitude as the delta prograded progressively more basinward (Fig. 20). The lower part of the A1 sequence represents an exception (Fig. 19). In this sequence, clinoform surfaces formed over a wider area, but are relatively low relief compared with those developed in younger sequences (Figs 15A and 16). This is caused by the available accommodation over the transgressed Klappmyss Formation: contrary to the

platform areas created during flooding of third-order sequences within the Kobbe Formation, there is enough accommodation to facilitate clinoform surfaces, but this accommodation is still less than what is available in front of discrete platform-edge breaks in each successive sequence.

Basinward of the parallel prodeltaic seismic reflectors, smaller-scale (100 to 150 m high) fourth-order clinoform surfaces show oblique and complex sigmoidal geometries. These fourth-order clinoform surfaces follow stratigraphically above and downlap onto third-order clinoform surfaces within each third-order sequence, and are interpreted to reflect stacked normal regressive prodelta lobes (for example, Figs 12 to 15). The fourth-order clinoforms have approximately the same basinward dip angle as the underlying third-order clinoforms. An apparent absence of topsets in the seismic data for the oblique and complex sigmoidal clinoform geometries observed in the fourth-order clinoforms (for example, Fig. 13C) could be interpreted to reflect restricted accommodation (e.g. Mitchum et al., 1977; Sangree & Widmier, 1977; Catuneanu et al., 2009). Such an interpretation could therefore imply bypass of some of the coarsest grained sediments available in the fluvial system to the delta front. Although the efficiency of bypass might be mitigated in delta plains over 1000 km wide, these oblique fourth-order clinoforms have therefore been suggested to represent discrete shelf-edge deltas with bypass of sandstone to the delta front at the maximum regressive stage of each third-order sequence (Glørstad-Clark et al., 2011). However, considering the lack of evidence for relative sea-level fall and the fine-grained sediment supplied to the basin (for example, Fig. 6), it is more likely that the oblique and complex sigmoidal clinoform surfaces result from an increase in sediment supply rates in combination with tuning effects at the interface between different clinoform surfaces and overlying deposits (Holgate et al., 2014; Patruno et al., 2015a) rather than relative sea-level change or changes in grain size.

The present study thus suggests that the clinoform surfaces in the Kobbe Formation are formed by two interconnected processes: (i) flooding of deltas in the underlying sequence creates a condensed and sediment starved series of third-order clinoform surfaces (Fig. 20A) which are interpreted to aggrade slowly in distal locations in response to limited influx of sediment distal to the prograding delta, but progressively faster as the shallow shelf is filled by sediments from the delta (Fig. 20B and C); and (ii) when the delta progrades across the platform-edge into deeper waters created by the underlying sequence, fourth-order clinoforms merge with the underlying third-order surfaces and prograde basinward together (Fig. 20D) before the cycle is repeated by the next MFS (Fig. 20E). Third-order clinoform surfaces thus

represent a flooding of the delta which is building fourth-order clinoform surfaces and also represents the basinward equivalent for the following fourth-order deltaic surfaces. The two orders of clinoform surfaces are distinct, but interconnected, and might therefore resemble compound clinoforms (Swenson et al., 2005). In the Kobbe Formation, however, the different scales of clinoform surfaces are created by changes in relative sea-level and progradation of these different clinoforms seems to be controlled by supply directly from the subaerial delta.

Clinoform geometries in this mud-dominated formation developed due to increased palaeobathymetric relief, and their development does not reflect a change in deposition within the delta topset or a fall in relative sea-level – promoting platform-edge deltas and bypass of sandstone. The prodeltaic deposits instead prograded at pace with, and were sourced from, a network of distributary channel systems on the contemporaneous delta.

Southern versus south-eastern sediment source

Reservoir quality in the central south-west Barents Sea is generally poor compared with the Goliat and Nucula discoveries along the southern margin (wells 7122/7-3 and 7125/4-1; Figs 1 and 5). Platform-edge delta interpretations implying sand bypass to the platform-edge and beyond have caused an overly optimistic prognosis for sandstone accumulation in the Kobbe Formation. Where reservoir scale sandstone deposits are encountered they are usually of poorer quality than the sandstone of the Goliat Field (Tsikalas et al., 2017). This is primarily due to how the more fine-grained, immature and mud-rich nature of sediments sourced from the south-east (Bergan & Knarud, 1993; Mørk, 1999; Eide et al., in press).

Nothing in the present seismic dataset can reveal the extent of sedimentary systems fed by the southern provenance area (for example, Fig. 21B), but it is likely that these systems would have linked with and fed into the south-easterly derived river systems in the Anisian/Ladinian. The relative contribution and extent of the more mature southern system could be investigated from petrography and provenance analysis (e.g. Fleming et al., 2016). This is beyond the scope of the current study, but the poor reservoir quality in the 7222/11-2 well (Fig. 6) indicates that the sediment contribution from the southern provenance area was negligible north of the Hammerfest Basin (*ca* 96 km from the margin, Fig. 21A).

Despite deeper burial and more immature mineralogy, there exists some reservoir potential in the basin interior. Mouth-bar deposits of FA3 in well 7222/11-2 show better reservoir properties (ϕ = 20%, K = 10 to 30 mD) than the channel sandstones of FA5 (ϕ = 18%, K = 2 to 8 mD) stratigraphically above (Fig. 6). This is due to coarser grained sediments with lower mud content deposited by more fluvial dominated processes. The texture of these deposits is more suitable for chlorite coating of grains which preserve pore space at depth (Line, 2015). Pore-preserving chlorite coating is also associated with favourable reservoir properties in fluvial channel belts in the overlying Snadd Formation (Henriksen et al., 2011; Line, 2015), and it is natural to consider that the sedimentary texture favouring pore-preserving chlorite coating in discrete mouth-bar deposits is related to similar depositional processes as more proximal fluvial river systems. On the contrary, the hydrodynamic regime which dominates tidally influenced distributary channel deposits favours deposition of finer grained sand and mud with chlorite clays as a limiting factor for permeability (Line, 2015). Reservoir properties of the south-easterly derived river system might therefore be expected to increase proximally towards its provenance area where the hydrodynamic regime favours a sedimentary texture that promotes pore-preserving chlorite coating.

Age constraints on sequences

Palynological data from Vigran et al. (2014) show relatively poor correlation to the sequences defined in seismic and well log data. The four sequences defined by Glørstad-Clark et al. (2011) have only three counterparts in this playnological zonation, two of which are found in the upper third-order A4 sequence. There are also large discrepancies between the palynological zonation in wells listed in the study by Vigran (2014) and the zonation in Paterson & Mangerud (2017). Furthermore, data from 7324/10-1 indicate an Olenekian age for the A1 sequence, which is not consistent with seismic and well log interpretations. This suggests that the relative age constraint on sequences and correlation of palynological zones within the Kobbe Formation needs to be scrutinized further.

DISCUSSION

Data and analysis presented above provides a better understanding of the depositional processes behind the mud-dominated clinoform successions of the Kobbe Formation of the Barents Sea, and provides a basis for comparing with and understanding similar deposits

worldwide. Clinoform development can be considered in terms of process regimes controlled both by autocyclic and allocyclic forcing factors, and three different stages of delta development are summarized schematically in Fig. 22, approximately to scale. Deltaic progradation occurred both on the platform (for example, Fig. 20B) and at the platform edge (for example, Fig. 20D) and was probably interrupted by transgressive events (for example, Figs 5 and 20A) in response to autocyclic avulsion. Large parts of the study area were prone to marine inundation and bay deposits in interfluve areas (for example, Fig. 7B). Southerly derived mature sediments probably formed alluvial fans close to the basin margin and fed tidally influenced channels merging with and forced westward by the easterly derived system across the Goliat Field (Fig. 7).

Frequent avulsions on the coastal plain were anticipated to have caused a uniform distribution of sediment in the clinoform topset, but despite extensive 3D seismic coverage (Fig. 16) no distributary channel systems are observed in the northern part of the present study area. Although this could be related to issues with seismic resolution in these surveys (Fig. 2A), well logs from this area are characterized by thin low gamma ray readings and no pronounced prodeltaic or deltaic sandstone deposits (Figs 8F and 11). This contrasts with well logs further south (Figs 3, 6 and 21), where channelized deposits are also observed in seismic closer to the platform edge (Fig. 16). Sediment accumulation in the absence of fluvial input in northern areas is interpreted to have been promoted by shore-parallel transport of suspended fine-grained sediment from a southern riverine input (Fig. 6G), contributing towards more linear platform-edge trends in these areas (Figs 16 and 18). Suspended sediments are readily redistributed by shear forces on the platform (cf. Pirmez et al., 1998; Ogston et al., 2000; Wright et al., 2001; Swenson et al., 2005) and are deposited basinward of the rollover (Wright et al., 1989; Friedrichs & Scully, 2007). Preferential deposition immediately basinward of the underlying rollover is seen at the maximum regressive stages of each sequence in the Kobbe Formation (Fig. 22C), but limited bottomset thickness in all sequences also indicates that the suspended sediments were not transported far basinward (Fig. 16).

Lateral transport of suspended sediment furthermore implies that the river mouth was detached from major parts of its widespread depocentre along the contemporaneous platform-edge (cf. Subaqueous Delta Clinoform in Walsh & Nittrouer, 2009), yet prodeltaic deposits recorded here suggest sediment supply directly from the river without a distinct staging area directly in front of the prograding system (Fig. 6I). As explained above, accumulation of fine-grained sediment on the prodeltaic platform and slope is therefore interpreted to have been

primarily facilitated by dilute low-density flows as seen in the frequent thin bedded turbidite deposits (Fig. 6H) in combination with contour currents (Fig. 6G) and additional fall-out from the hypopycnal component of sedimentary plumes from the distributary systems effluent (Wright et al., 1988; Fig. 22B). Basinward protrusions in the thickness trends of the A3 and A4 sequences (Fig. 16C and D) also attest to this mixture of prodelta accumulation and significant longshore drift. Protrusions formed where platform-edge deltas deposited preferentially more sediment directly in front of the delta than was redistributed longshore (cf. Proximal Accumulation Dominated in Walsh & Nittrouer, 2009), causing the platform-edge to prograde further basinward in the south relative to the Hoop Fault Complex area further north.

There is a clear and documented eustatic signal at the stage level (Miller et al., 2005), separating the Kobbe Formation from overlying and underlying formations (Glørstad-Clark et al., 2010). In the Anisian, four upward shallowing sequences have also been observed in other basins (e.g. Gianolla et al., 1998; Embry, 2011) and the maximum flooding surfaces that separate the distinct third-order sequences of Glørstad-Clark et al. (2011) might thus represent a eustatic signal. Despite a significant difference in scale, both shelf-edge and platform-edge deltas might form without a fall in relative sea-level if sediment supply is sufficient (Burgess & Hovius, 1998; Carvajal & Steel, 2006; Carvajal et al., 2009), and it is fair to assume that the smaller-scale platform-edge deltas studied herein prograded faster and developed more rapidly compared with larger-scale shelf-edge equivalents (cf. Patruno et al., 2015a). Relatively low rates of eustatic sea-level change are furthermore promoted by the prevailing Triassic Greenhouse climatic setting (Sømme et al., 2009), which facilitated a relatively stable high-accommodation setting in which syn-sedimentary compaction and subsidence in the deltaic topset could add to the accommodation. In addition to this, a gentle delta gradient (Fig. 19) impeded transport of coarse-grained sediment to the delta front and basin. The delta front thus remained relatively fine-grained and heterolithic even at discrete maximum regressive stages (Fig. 20D).

Clinoform surfaces in the Kobbe Formation are therefore interpreted to represent normal regressive mud-dominated platforms with a generally linear advance facilitated by longshore currents (Fig. 22) accompanied by subtle protrusions at discrete sites of platform-edge deltas (Fig. 16). Uniform and shallow water depths on the transgressed platforms probably facilitated a more even distribution of prodeltaic sediments (e.g. Plint, 2014), preventing discrete clinoform surfaces from forming (Fig. 21B). During progradation, continuous

deposition at the delta front counteracted formation of deep, long-lived prodeltaic canyons on the platform and at the platform-edge, instead promoting relatively thin chute channels and multiple, unconstrained, thin low-density turbidite aprons on the slope (cf. Plink-Björklund et al., 2001; Dixon et al., 2012) which might have been reworked by longshore currents (cf. Rebesco et al., 2014). This explains the distinct lack of seismically resolvable turbidite channels, while the presence of sporadic prodeltaic turbidite deposits (for example, Fig. 6I) suggest episodic hyperpycnal flows from distributary channels in the Kobbe Formation (cf. Lamb & Mohrig, 2009; Lamb et al., 2010).

The present case-study demonstrates that shallow marine and prodeltaic deposits in high-accommodation, mud-dominated successions are generally fine-grained and highly heterolithic. Only minor sandstone deposits have been observed within the clinoform successions, and these heterogeneities are primarily the result of autocyclic changes where the limited sandstone input hinges on the presence of distributary channels which diminish in volume proximal to the platform-edge delta. Reservoir-scale sandstone accumulations are restricted to these distributary channels, and their reservoir properties are most favourable in the proximal parts of the basin, either due to more mature provenance areas (as seen along the southern margin of the basin, Fig. 7) or sedimentary textures favourable for pore-preserving chlorite coating (as seen in the more fluvial dominated mouth-bar deposits in well 7222/11-2, Fig. 6).

Fourth-order clinoform geometries are interconnected with more distal third-order clinoform surfaces and develop in response to underlying bathymetry. Fourth-order clinoforms are therefore encountered both in areas with and without indications for platform-edge deltas (Figs 15D, 16 and 17) and the transition from third to fourth-order clinoform geometries simply records the gradual filling of accommodation space and does not necessarily reflect influx of sandstone to the delta front or basin.

CONCLUSIONS

Clinoform successions in the mud-dominated Kobbe Formation consist predominantly of siltstone deposited by contour currents interbedded with thin bedded dilute turbidite beds, but also comprise sporadic prodeltaic turbidite sandstone sheets below seismic resolution. These deposits are interpreted to be sourced directly from the delta front either on the platform or at the platform-edge in response to normal regressive delta progradation. Contemporaneous shore-parallel transport of suspended sediments facilitated deposition in areas without pronounced channel networks and has resulted in widespread, linear platform edges. Deltaic topsets show heterogeneous deposits which follow a predictable pattern towards less marine influenced deposits in proximal parts of the delta plain.

Normal regressive progradation and heterolithic marine-influenced topset deposits indicate a high accommodation setting. In such a scenario, there are few mechanisms favouring bypass of coarse-grained material to the delta front and the best reservoir rocks are therefore expected in the upper delta plain regions. Because of this sequestration and continual topset accumulation, there are no direct relationships between oblique clinoform surfaces or areas of increased isopach thickness and preferential sandstone accumulations in the Kobbe Formation. However, more favourable reservoir properties are present in certain depositional environments (i.e. in fluvial deposits prone to favourable chlorite coating which preserve porosity and permeability during burial), and in general along the southern margin due to shallower burial and a local, more mature source area.

Clinoform geometries formed in response to progradation of the mud-dominated delta across the platform-edge of the underlying sequence and are thus the result of inherited bathymetry rather than reflecting autogenic changes from mud-dominated to sand-dominated prodelta. The transition from sigmoidal third-order clinoform surfaces to oblique and complex sigmoidal fourth-order clinoform surfaces at discrete maximum regressive stages is caused by increased sedimentation rates as the delta progrades across its underlying platform edge, without changes in grain size or relative sea-level. Changes in geometries thus represent the gradual transition between two interconnected depositional systems.

ACKNOWLEDGEMENTS

This work has been funded by the Triassic North project under grant 234152 from the Research Council of Norway (RCN) and with financial support from Statoil, Lundin, Tullow Oil Norway, Edison Norway and DEA Norway. We also wish to thank Point Resources (formerly Rocksource) for supporting part of this work. TGS-Nopec, the Norwegian Petroleum Directorate and Spectrum are thanked for letting us use 2D and 3D seismic data, and Schlumberger for academic software licenses. Reidar Müller, Zhiyuan Ge and Takemi Murase are thanked for thought-provoking discussions, and Niall William Paterson is kindly thanked for reading through the manuscript. Ingrid Anell, an anonymous reviewer and Piret Plink-Björklund are gratefully acknowledged for many excellent suggestions which improved the quality and clarity of the manuscript considerably.

REFERENCES

Anell, I., Midtkandal, I. and Braathen, A. (2014) Trajectory analysis and inferences on geometric relationships of an Early Triassic prograding clinoform succession on the northern Barents Shelf. Mar. Petrol. Geol., 54, 167-179.

Baig, I., Faleide, J.I., Jahren, J. and Mondol, N.H. (2016) Cenozoic exhumation on the southwestern Barents Shelf: Estimates and uncertainties constrained from compaction and thermal maturity analyses. Mar. Petrol. Geol., 73, 105-130.

Bergan, M. and Knarud, R. (1993) Apparent changes in clastic mineralogy of the Triassic-Jurassic succession, Norwegian Barents Sea: Possible implications for palaeodrainage and subsidence. In: Arctic Geology and Petroleum Potential (Eds T.O. Vorren, E. Bergsager, Ø.A.

Dahl-Stamnes, E. Holter, B. Johansen, E. Lie, T.B. Lund), Norw. Petrol. Soc. Spec. Publ., 2, 481–493, Elsevier, Amsterdam.

Bhattacharya, J.P. and MacEachern, J.A. (2009) Hyperpycnal rivers and prodeltaic shelves in the Cretaceous seaway of North America. J. Sed. Res., 79, 184-209.

Blum, M.D. and Törnqvist, T.E. (2000) Fluvial responses to climate and sea-level change: a review and look forward. Sedimentology, 47, 2-48.

Bridge, J.S. (2006) Fluvial facies models: recent developments. SEPM Spec. Publ., 84, 85 p.

Brown, A.R. (2004) Interpretation of three-dimensional seismic data. AAPG Mem. 42, 646.

Bugge, T., Elvebakk, G., Fanavoll, S., Mangerud, G., Smelror, M., Weiss, H.M., Gjelberg, J., Kristensen, S.E. and Nilsen, K. (2002) Shallow stratigraphic drilling applied in hydrocarbon exploration of the Nordkapp Basin, Barents Sea. Mar. Petrol. Geol. 19, 13-37.

Burgess, P.M. and Hovius, N. (1998) Rates of delta progradation during highstands: consequences for timing of deposition in deep-marine systems. J. Geol. Soc., 155, 217-222.

Burpee, A.P., Slingerland, R.L., Edmonds, D.A., Parsons, D., Best, J., Cederberg, J., McGuffin, A., Caldwell, R., Nijhuis, A. and Royce, J. (2015) Grain-Size Controls On the Morphology and Internal Geometry of River-Dominated Deltas. J. Sed. Res., 85, 699-714.

Carter, D.C. (2003) 3-D seismic geomorphology: Insights into fluvial reservoir deposition and performance, Widuri field, Java Sea. AAPG Bull., 87, 909-934.

Carvajal, C., Steel, R. and Petter, A. (2009) Sediment supply: the main driver of shelf-margin growth. Earth-Sci. Rev. 96, 221-248.

Carvajal, C.R. and Steel, R.J. (2006) Thick turbidite successions from supply-dominated shelves during sea-level highstand. Geology, 34, 665-668.

Castagna, J.P. (1993) Petrophysical imaging using AVO. Lead. Edge, 12, 172-178.

Castagna, J.P., Sun, S. and Siegfried, R.W. (2003) Instantaneous spectral analysis: Detection of low-frequency shadows associated with hydrocarbons. Lead. Edge, 22, 120-127.

Castagna, J.P. and Sun, S. (2006) Comparison of spectral decomposition methods. First break, 24, 75–79.

Catuneanu, O., Abreu, V., Bhattacharya, J.P., Blum, M.D., Dalrymple, R.W., Eriksson, P.G., Fielding, C.R., Fisher, W.L., Galloway, W.E., Gibling, M.R. and Giles, K.A. (2009) Towards the standardization of sequence stratigraphy. Earth-Sci. Rev., 92, 1-33.

Clifton, H.E. (2006) A Reexamination of facies models for clastic shorelines. In: Facies Models Revisited (Eds H.W. Posamentier and R.G. Walker), SEPM Spec. Publ., 24, 126–184.

Coleman, J.M., Gagliano, S.M. and Webb, J.E. (1964) Minor sedimentary structures in a prograding distributary. Marine Geology, 1, 240-258.

Dalland, A., Worsley, D. and Ofstad, K. (1988) A lithostratigraphic scheme for the Mesozoic and Cenozoic succession offshore mid- and northern Norway. Norw. Petrol. Direct. Bull., 4, 65.

Diessel, C.F. (2007) Utility of coal petrology for sequence-stratigraphic analysis. International J. Coal Geol., 70, 3-34.

Dixon, J.F., Steel, R.J. and Olariu, C. (2012) Shelf-edge delta regime as a predictor of deep-water deposition. J. Sed. Res., 82, 681-687.

Eide, C.H., Klausen, T.G., Katkov, D., Suslova, A.A. and Helland-Hansen, W. (In press) Linking an Early Triassic delta to antecedent topography: source-to-sink study of the southwestern Barents Sea margin. Geol. Soc. Am. Bull.

Embry, A. (2011) Petroleum prospectivity of the Triassice-Jurassic succession of Sverdrup Basin, Canadian Arctic Archipelago. In: Arctic Petroleum Geology (Eds A.M. Spencer, A.F. Embry, D.L. Gautier, A.V. Stoupakova and K. Sørensen), Geol. Soc. Mem., 35, 545-558.

Faleide, J., Vågnes, E. and Gudlaugsson, S. (1993) Late Mesozoic–Cenozoic evolution of the southwestern Barents Sea. Mar. Petrol. Geol., 10, 186–214.

Faleide, J.I., Solheim, A., Fiedler, A., Hjelstuen, B.O., Andersen, E.S. and Vanneste, K. (1996) Late Cenozoic evolution of the western Barents Sea-Svalbard continental margin. Global Planet. Change, 12, 53–74.

Frazier, D.E. (1967) Recent deltaic deposits of the Mississippi River: their development and chronology. Trans. Gulf Coast Assoc. Geol. Soc. 17, 287–315.

Friedrichs, C.T. and Scully, M.E. (2007) Modeling deposition by wave-supported gravity flows on the Po River prodelta: from seasonal floods to prograding clinoforms. Cont. Shelf Res., 27, 322-337.

Flemming, B.W. (2012) Siliciclastic back-barrier tidal flats. In: Principles of Tidal Sedimentology (Eds R.A. Davis, Jr., R.W. Dalrymple), Springer Netherlands, 231-267.

Fleming, E.J., Flowerdew, M.J., Smyth, H.R., Scott, R.A., Morton, A.C., Omma, J.E., Frei, D. and Whitehouse, M.J. (2016) Provenance of Triassic sandstones on the southwest Barents Shelf and the implication for sediment dispersal patterns in northwest Pangaea. Mar. Petrol. Geol., 78, 516-535.

Gabrielsen, R.H., Færseth, R.B., Jensen, L.N., Kalheim, J.E. and Riis, F. (1990) Structural elements of the Norwegian continental shelf part I: the Barents Sea region. Norw. Petrol. Direct. Bull., 6, 47.

Galloway, W.E. (1975) Process framework for describing the morphologic and stratigraphic evolution of deltaic depositional systems. In: Deltas: Models for Exploration (Ed M.L. Broussard), Houston Geological Society, Houston, pp. 87-98.

Galloway, W.E. (1998) Siliciclastic slope and base-of-slope depositional systems: component facies, stratigraphic architecture, and classification. AAPG Bull., 82, 569-595.

Gianolla, P., De Zanche V. and Mietto, P. (1998) Triassic sequence stratigraphy in the Southern Alps (Northern Italy): definition of sequences and basin evolution. In: Mesozoic and Cenozoic Sequence Stratigraphy of European Basins (Eds P.C. de Graciansky, J. Hardenbol, T. Jacquin and P.R. Vail), SEPM Spec. Publ., 60, 719–747.

Glørstad-Clark, E., Faleide, J.I., Lundschien, B.A. and Nystuen, J.P. (2010) Triassic seismic sequence stratigraphy and paleogeography of the western Barents Sea area. Mar. Petrol. Geol., 27, 1448–1475.

Glørstad-Clark, E., Birkeland, E.P., Nystuen, J.P., Faleide, J.I. and Midtkandal, I. (2011) Triassic platform-margin deltas in the western Barents Sea. Mar. Petrol. Geol., 28, 1294–1314.

Gong, C., Steel, R.J., Wang, Y., Lin, C. and Olariu, C. (2016) Shelf-margin architecture variability and its role in sediment-budget partitioning into deep-water areas. Earth Sci. Rev., 154, 72-101.

Hartley, A.J., Weissmann, G.S. and Scuderi, L. (2017) Controls on the apex location of large deltas. J. of the Geol. Soc., 174, 10-13.

Helland-Hansen, W., Steel, R.J. and Sømme, T.O. (2012) Shelf genesis revisited. J. Sed. Res., 82, 133-148.

Henriksen, E., Ryseth, A.E., Larssen, G.B., Heide, T., Rønning, K., Sollid, K. and Stoupakova, A.V. (2011) Chapter 10: Tectonostratigraphy of the greater Barents Sea: implications for petroleum systems. Geol. Soc. London Mem., 35, 163–195.

Holgate, N.E., Hampson, G.J., Jackson, C.A.L. and Petersen, S.A. (2014) Constraining uncertainty in interpretation of seismically imaged clinoforms in deltaic reservoirs, Troll field, Norwegian North Sea: Insights from forward seismic models of outcrop analogs. AAPG Bull., 98, 2629-2663.

Klausen, T.G., Ryseth, A.E., Helland-Hansen, W., Gawthorpe, R. and Laursen, I. (2014) Spatial and temporal changes in geometries of fluvial channel bodies from the Triassic Snadd Formation of offshore Norway. J. Sed. Res., 84, 567–585.

Klausen, T.G., Ryseth, A.E., Helland-Hansen, W., Gawthorpe, R. and Laursen, I. (2015) Regional development and sequence stratigraphy of the Middle to Late Triassic Snadd Formation, Norwegian Barents Sea. Mar. Petrol. Geol., 62, 102–122.

Lamb, M.P. and Mohrig, D. (2009) Do hyperpycnal-flow deposits record river-flood dynamics?. Geology, 37, 1067-1070.

Lamb, M.P., McElroy, B., Kopriva, B., Shaw, J. and Mohrig, D. (2010) Linking river-flood dynamics to hyperpycnal-plume deposits: Experiments, theory, and geological implications. Geol. Soc. Am. Bull., 122, 1389-1400.

Lamb, M.P., Nittrouer, J.A., Mohrig, D. and Shaw, J. (2012) Backwater and river plume controls on scour upstream of river mouths: Implications for fluvio-deltaic morphodynamics. J. Geophys. Res.: Earth Surface, 117(F1).

Laugier, F.J. and Plink-Björklund, P. (2016) Defining the shelf edge and the three-dimensional shelf edge to slope facies variability in shelf-edge deltas. Sedimentology, 63, 1280-1320.

Line, L.H. (2015) Reservoir characterization of the Middle-Upper Triassic Kobbe and Snadd Formations in the southwestern Barents Sea: The role of chlorite coating (Master's thesis). University of Oslo, http://urn.nb.no/URN:NBN:no-53449.

Liu, J. and Marfurt, K.J. (2007) Instantaneous spectral attributes to detect channels. Geophysics, 72, P23-P31.

Lundschien, B.A., Høy, T. and Mørk, A. (2014) Triassic Hydrocarbon Potential in the Northern Barents Sea; integrating Svalbard and stratigraphic core data. Norw. Petrol. Direct. Bull., 11, p. 3-20, Stavanger, ISBN 978-82-7257-117-6.

Mack, G.H., James, W.C. and Monger, H.C. (1993) Classification of paleosols. Geol. Soc. Am. Bull., 105, 129-136.

Martinius, A.W. and Van den Berg, J.H. (2011) Atlas of Sedimentary Structures in Estuarine and Tidally-Influenced River Deposits of the Rhine-Meuse-Scheldt System. EAGE Publications BV, Houten, 298 pp.

Miller, K.G., Kominz, M.A., Browning, J.V., Wright, J.D., Mountain, G.S., Katz, M.E., Sugarman, P.J., Cramer, B.S., Christie-Blick, N. and Pekar, S.F. (2005) The Phanerozoic record of global sea-level change. Science, 310, 1293-1298.

Mitchum Jr, R.M., Vail, P.R. and Sangree, J.B., 1977. Seismic stratigraphy and global changes of sea level, Part 6: Stratigraphic interpretation of seismic reflection patterns in depositional sequences. In: Seismic Stratigraphy: Applications to Hydrocarbon Exploration (Ed C.E. Payton), AAPG Mem., 26, 117–133.

Mulder, T., Syvitski, J.P., Migeon, S., Faugères, J.C. and Savoye, B. (2003) Marine hyperpycnal flows: initiation, behavior and related deposits. A review. Mar. Petrol. Geol., 20, 861-882.

Mørk, M.B.E. (1999) Compositional variations and provenance of Triassic sandstones from the Barents Shelf. J. Sed. Res. 69, 690-710.

Mørk, A. and Elvebakk, G. (1999) Lithological description of subcropping Lower and Middle Triasic rocks from the Svalis Dome, Barents Sea. Polar Res. 18, 83-104.

Mørk, A., Dallmann, W.K., Dypvik, H., Johannessen, E.P., Larssen, G.B., Nagy, J., Nøttvedt, A., Olaussen, S., Pchelina, T.M. and Worsley, D. (1999) Mesozoic lithostratigraphy. In: Lithostratigraphic Lexicon of Svalbard. Review and Recommendations for Nomenclature Use. Upper Palaeozoic to Quaternary bedrock (Ed W.K. Dallmann), pp. 127–214. Norsk Polarinstitutt, Tromsø.

Nemec, W. (1995) The dynamics of deltaic suspension plumes. Geology of deltas, 31-93, A.A. Balkema, Rotterdam.

Ogston, A.S., Cacchione, D.A., Sternberg, R.W. and Kineke, G.C. (2000) Observations of storm and river flood-driven sediment transport on the northern California continental shelf. Cont. Shelf Res., 20, 2141-2162.

Olariu, C. and Bhattacharya, J.P. (2006) Terminal distributary channels and delta front architecture of river-dominated delta systems. J. Sed. Res., 76, 212-233.

Orton, G.J. and Reading, H.G. (1993) Variability of deltaic processes in terms of sediment supply, with particular emphasis on grain size. Sedimentology, 40, 475-512.

Ostrander, W. (1984) Plane-wave reflection coefficients for gas sands at nonnormal angles of incidence. Geophysics, 49, 1637-1648.

Paterson, N.W. and Mangerud, G. (2017) Palynology and depositional environments of the Middle – Late Triassic (Anisian – Rhaetian) Kobbe, Snadd and Fruholmen formations, southern Barents Sea, Arctic Norway. Mar. Petrol. Geol., 86, 304-324.

Patruno, S., Hampson, G.J. and Jackson, C.A. (2015a) Quantitative characterisation of deltaic and subaqueous clinoforms. Earth Sci. Rev. 142, 79-119.

Patruno, S., Hampson, G.J., Jackson, C.A.L. and Dreyer, T. (2015b) Clinoform geometry, geomorphology, facies character and stratigraphic architecture of a sand-rich subaqueous delta: Jurassic Sognefjord Formation, offshore Norway. Sedimentology, 62, 350-388.

Pirmez, C., Pratson, L.F. and Steckler, M.S. (1998) Clinoform development by advection-diffusion of suspended sediment: Modeling and comparison to natural systems: J. Geoph. Res., 103, 24-141.

Plink-Björklund, P., Mellere, D. and Steel, R.J. (2001) Turbidite variability and architecture of sand-prone, deep-water slopes: Eocene clinoforms in the Central Basin, Spitsbergen. J. Sed. Res., 71, 895-912.

Plink-Björklund, P. and Steel, R.J. (2004) Initiation of turbidity currents: outcrop evidence for Eocene hyperpycnal flow turbidites. Sed. Geol., 165, 29-52.

Plint, A.G. (2014) Mud dispersal across a Cretaceous prodelta: storm-generated, wave-enhanced sediment gravity flows inferred from mudstone microtexture and microfacies. Sedimentology, 61, 609-647.

Porębski, S.J. and Steel, R.J. (2003) Shelf-margin deltas: their stratigraphic significance and relation to deepwater sands. Earth Sci. Rev., 62, 283-326.

Posamentier, H.W. (2001) Lowstand alluvial bypass systems: incised vs. unincised. AAPG Bull., 85, 1771-1793.

Poyatos-Moré, M., Jones, G.D., Brunt, R.L., Hodgson, D.M., Wild, R.J. and Flint, S.S. (2016) Mud-Dominated Basin-Margin Progradation: Processes and Implications: J. Sed. Res., 86, 863-878.

Rasmussen, A., Kristensen, S.E., Van Veen, P.M., Stolan, T. and Vail, P.R. (1993) Use of sequence stratigraphy to define a semi-stratigraphic play in Anisian sequences, southwestern Barents Sea. In: Arctic Geology and Petroleum Potential (Eds T.O. Vorren, E. Bergsager, Ø.A. Dahl-Stamnes, E. Holter, B. Johansen, E. Lie, T.B. Lund), Norw. Petrol. Soc. Spec. Publ., 2, 439-455, Elsevier, Amsterdam.

Rebesco, M., Hernández-Molina, F.J., Van Rooij, D. and Wåhlin, A. (2014) Contourites and associated sediments controlled by deep-water circulation processes: state-of-the-art and future considerations. Mar. Geol., 352, 111-154.

Rich, J.L. (1951) Three critical environments of deposition, and criteria for recognition of rocks deposited in each of them: Geol. Soc. Am. Bull., 62, 1-20.

Riis, F., Lundschien, B.A., Høy, T., Mørk, A. and Mørk, M.B.E. (2008) Evolution of the Triassic shelf in the northern Barents Sea region. Polar Res., 27, 318–338.

Rossi, V.M., Kim, W., López, J.L., Edmonds, D., Geleynse, N., Olariu, C., Steel, R.J., Hiatt, M. and Passalacqua, P. (2016) Impact of tidal currents on delta-channel deepening, stratigraphic architecture, and sediment bypass beyond the shoreline. Geology, 44, 927-930.

Ryan, M.C., Helland-Hansen, W., Johannessen, E.P. and Steel, R.J. (2009) Erosional vs. accretionary shelf margins: the influence of margin type on deepwater sedimentation: an example from the Porcupine Basin, offshore western Ireland. Basin Res., 21, 676-703.

Ryseth, A. (2014) Sedimentation at the Jurassic-Triassic boundary, south-west Barents Sea. In: From Depositional Systems to Sedimentary Successions on the Norwegian Continental Margin (Eds A.W. Martinius, R. Ravnås, J.A. Howell, R.J. Steel, and J.P. Wonham), Int. Assoc. Sedimentol. Spec. Publ., 46, 187-214.

Sangree, J.B. and Widmier, J.M. (1977) Seismic stratigraphy and global changes in sea level, Part 9, Seismic interpretation of clastic depositional facies. In: Seismic Stratigraphy: Applications to Hydrocarbon Exploration (Ed C.E. Payton), AAPG Mem., 26, 165–184.

Schieber, J. and Southard, J.B. (2009) Bedload transport of mud by floccule ripples—Direct observation of ripple migration processes and their implications. Geology, 37, 483-486.

Shanmugam, G. 2012. New perspectives on deep-water sandstones: origin, recognition, initiation and reservoir quality. Handbook of Petroleum Exploration and Production, Volume 9, Elsevier, Amsterdam, p. 524.

Skjold, L.J., van Veen, P.M., Kristensen, S.E., and Rasmussen, A.R. (1998) Triassic sequence stratigraphy of the southwestern Barents Sea. In: Mesozoic and Cenozoic Sequence Stratigraphy of European Basins (Eds P.C. de Graciansky, J. Hardenbol, T. Jacquin, P.J.

Vail), Society for Sedimentary Geology, Special Publication Society for Sedimentary Geology, No. 60. SEPM, Tulsa, 651-666.

Slingerland, R. and Smith, N.D. (2004) River avulsions and their deposits. Annu. Rev. Earth Planet. Sci., 32, 257-285.

Steel, R.J., Porebski, S.J., Plink-Bjorklund, P., Mellere, D. and Schellpeper, M. (2003) Shelf-edge delta types and their sequence-stratigraphic relationships. In: Shelf Margin Deltas and Linked Down Slope Petroleum Systems (Eds H.R. Roberts, N.C. Rosen, R.H. Fillon, J.B. Anderson), 23rd Annual Gulf Coast Section SEPM, 205-230.

Stow, D.A., Howell, D.G. and Nelson, C.H. (1983) Sedimentary, tectonic, and sea-level controls on submarine fan and slope-apron turbidite systems. Geo-Mar. Lett., 3, 57-64.

Swenson, J.B., Paola, C., Pratson, L., Voller, V.R. and Murray, A.B. (2005) Fluvial and marine controls on combined subaerial and subaqueous delta progradation: Morphodynamic modeling of compound-clinoform development. J. Geoph. Res.: Earth Surface, 110(F2).

Sydow, J. and Roberts, H.H. (1994) Stratigraphic framework of a late Pleistocene shelf-edge delta, northeast Gulf of Mexico. AAPG Bull., 78, 1276-1312.

Sylvester, Z., Deptuck, M.E., Prather, B.E., Pirmez, C. and O'Byrne, C. (2012) Seismic stratigraphy of a shelf-edge delta and linked submarine channels in the northeastern Gulf of Mexico. In: Application of the Principles of Seismic Geomorphology to Continental-Slope and Base-of-Slope Systems: Case Studies from Seafloor and Near-Seafloor Analogues (Eds B.E. Prather, M.E. Deptuck, D. Mohrig, B.V. Hoorn, R.B. Wynn), SEPM Spec. Publ., 99, 31-59.

Syvitski, J.P. and Saito, Y. (2007) Morphodynamics of deltas under the influence of humans. Global and Planet. Change, 57, 261-282.

Sømme, T.O., Helland-Hansen, W. and Granjeon, D. (2009) Impact of eustatic amplitude variations on shelf morphology, sediment dispersal, and sequence stratigraphic interpretation: icehouse versus greenhouse systems. Geology 37, 587-590.

Tsikalas, F., Blackley, C., Alzeni, F., Van Noorden M., Uncini, G., Farrer G. and Mavilla, N. (2017) Kobbe Formation reservoir potential outside Hammerfest Basin in the light of Aurelia (7222/1-1) well results. Abstract Arctic Energy Conference 2017, Svolvær (Lofoten), 29-30 May.

Vigran, J.O., Mangerud, G., Mørk, A., Worsley, D. and Hochuli, P.A. (2014) Palynology and Geology of the Triassic Succession on Svalbard and the Barents Sea. Geol. Surv. Norw. Spec. Publ., 14, 272 pp., Trondheim, ISBN 978-82-7385-156-7.

van Veen, P.M., Skjold, L.J., Kristensen, S.E., Rasmussen, A., Gjelberg, J. and Stølan, T. (1993) Triassic sequence stratigraphy in the Barents Sea. In: Arctic Geology and Petroleum Potential (Eds T.O. Vorren, E. Bergsager, Ø.A. Dahl-Stamnes, E. Holter, B. Johansen, E. Lie, T.B. Lund), Norw. Petrol. Soc. Spec. Publ., 2, 515-538, Elsevier, Amsterdam.

Walsh, J.P. and Nittrouer, C.A. (2009) Understanding fine-grained river-sediment dispersal on continental margins. Mar. Geol., 263, 34-45.

Weitschat, W. and Dagys, A.S. (1989) Triassic biostratigraphy of Svalbard and a comparison with NE-Siberia. Mitt. Geol.-Paläont. Inst. Univ. Hamburg 68, 179–213.

Widess, M.B. (1973) How thin is a thin bed, Geophysics, 38, 1176-1180.

Wood, R.J., Edrich, S.P. and Hutchinson, I. (1989) Influence of North Atlantic Tectonics on the Large-Scale Uplift of the Stappen High and Loppa High, Western Barents Shelf: Chapter 36: North Sea and Barents Shelf. In: Extensional Tectonics and Stratigraphy of the North Atlantic Margins (Eds A.J. Tankard, and H.R. Balkwill), AAPG Mem., 46, 559-566.

Worsley, D. (2008) The post-Caledonian development of Svalbard and the western Barents Sea. Polar Res. 27, 298-317.

Wright, L.D., Friedrichs, C.T., Kim, S.C. and Scully, M.E. (2001) Effects of ambient currents and waves on gravity-driven sediment transport on continental shelves. Mar. Geol., 175, 25-45.

Wright, L.D. (1989) Dispersal and deposition of river sediments in coastal seas: models from Asia and the tropics. Neth. J. Sea Res., 23, 493-500.

Wright, L.D., Wiseman, W.J., Bornhold, B.D., Prior, D.B., Suhayda, J.N., Keller, G.H., Yang, Z.S. and Fan, Y.B. (1988) Marine dispersal and deposition of Yellow River silts by gravity-driven underflows. Nature, 332, 629-632.

FA	Gross lithology	Characteristics	Dimensions	Facies	Interpretation	Figs
1	Organic rich mudstone	High gamma-ray readings and high amplitude in seismic. This facies has not been cored in the Kobbe Formation, shallow stratigraphic drilling sampled equivalent deposits showing organic content up to 8% (Mørk & Elvebakk, 1999). Followed conformably by FA2	A few metres thick proximally (7222/11-2), but as much as 20 m distally	Organic shale	**Offshore**	5B
2	Siltstone	Moderate gamma ray values. In core, structureless grey siltstone and flocculated mudstone with *Planolites,* shell debris, carbonate cemented horizons and few phosphorite nodules	Range from 6 to 8 m down to a few centimetres in	Silt and floc.mud	**Prodelta**	6F, G, H
	Very fine sandstone	Low gamma ray. Planar parallel lamination with scours and graded top to siltstone in discrete Bouma Tb-d or Ta-b sequences. *Planolites, Skolithos* and *Teichicnus* occur	2 to 50 cm thick. Some stacked in 8.6 m thick units	Turbidite deposits		6I
	Very inef sandstone	Low gamma ray. Lense-shaped sst beds with irregular, scoured bases and millimetre-scale planar sandstone interbedded with siltstone. Rare beds with cross-lamination and	Millimetres to 10 cm in thickness in core from	Contourite		6G, H
3	Very fine to fine	Erratic but generally low gamma ray. Wavy to flaser bedded sandstone interbedded with mud drapes, fluid mud deposits and reactivation surfaces. Sparse bioturbation, *Planolites*	30 cm to 1.5 m thick beds	Tidal flat	**Shallow marine**	7F
	Fine-grained sandstone	Low gamma ray. Chaotic and irregular lamination highlighted by carbonaceous material along bedding planes. Also unidirectional cross-lamination, but no bioturbation	2.4 m in thickness in 7222/11-2	Mouth bar		6E
	Fine to very fine	Low gamma ray. Planar parallel lamination and bidirectional cross-lamination. Relatively diverse and intense bioturbation, *Planolites Teichicnus, Skolithos, Diplocraterion* and shell frag.	1 to 4 m in thickness	Shoreface/transgressive lag		6E
4	Coal/organic rich siltstone	Low gamma ray, high neutron. Coal and carbonaceous siltstone and mudstone with root traces and organic debris. Commonly gradational contact to mottled siltstone, sharp contact	2 to 15 cm in 7230/05-U-05 and 7230/05-U-06	Coal and carbonate.	**Coastal plain**	6F, 8C
	Mudstone to siltstone,	Moderate gamma ray. Clay aggregates and mottled siltsone with greenish-white to reddish colour, varying between vertisol and histosol. Root traces and siderite nodules are common	10 cm to 6 m in 7230/05-U-05 and 7230/05-U-06	Palaeosol		8E
	Siltstone with very fine to	Moderate to low gamma ray. Grey siltsone interbedded with sandstone often in upward coarsening trends and unidirectional cross lamination Intense to moderate bioturbation,	2 to 4 m upward coarsening trends	Bay fill		6D, 7B
5	Fine-grained sandstone, grey siltstone	Low gamma ray with spikes of higher values. Fine-grained sandstone with siltstone interbeds and mudstone draping foresets. Siltstone also abundantly present as angular rip-up clasts and fluid muds. *Planolites* biroturbation. Erosive base, but often heterolithic lower part	Up to 19 m thick in 7222/11-2. 100 m to 5 km wide	Tidally influenced channel	**Channel belts**	6B, C; 5C, D; 8B
	Fine to medium	Low gamma ray. Unidirectional cross-lamination or chatoic lamination, some fine-grained material highlighting bedding planes. Plant debris common, rare concretions. Erosive base	10 m in 7122/7-3	Fluvial channel		7C

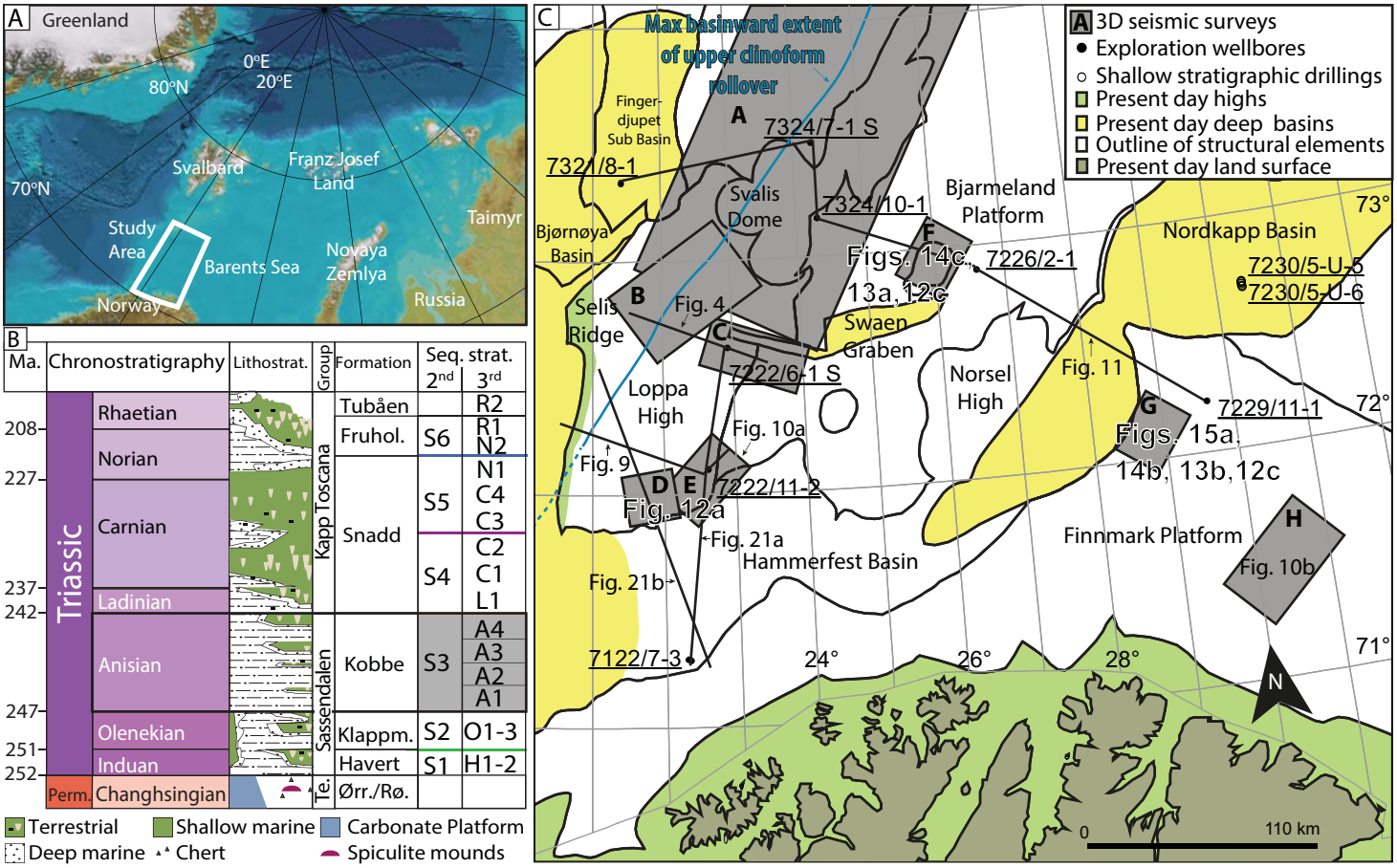

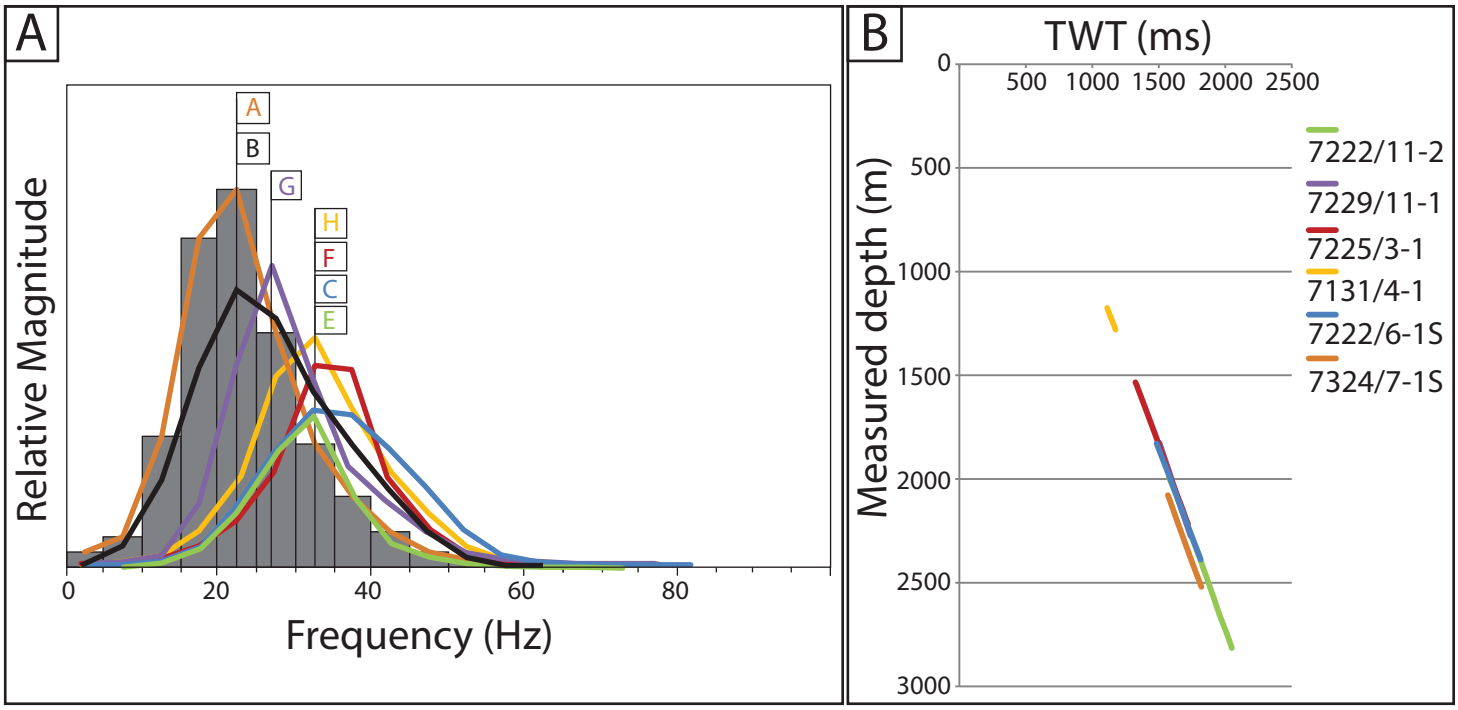

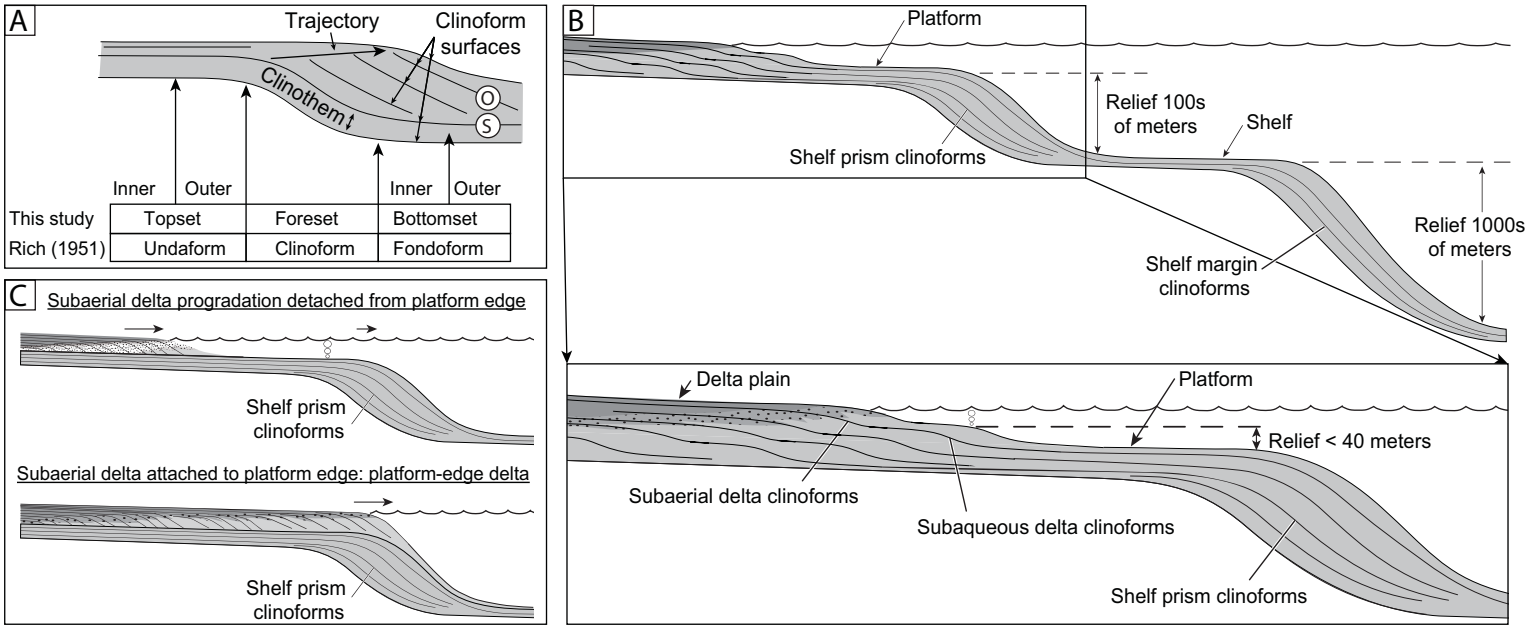
A
Trajectory
Clinoform surfaces
Clinothem
O
S
Inner
Outer
Inner
Outer
This study
Topset
Foreset
Bottomset
Rich (1951)
Undaform
Clinoform
Fondoform
B
Platform
Relief 100s of meters
Shelf
Shelf prism clinoforms
Relief 1000s of meters
Shelf margin clinoforms
Delta plain
Platform
Relief < 40 meters
Subaerial delta clinoforms
Subaqueous delta clinoforms
Shelf prism clinoforms
C
Subaerial delta progradation detached from platform edge
Shelf prism clinoforms
Subaerial delta attached to platform edge: platform-edge delta
Shelf prism clinoforms

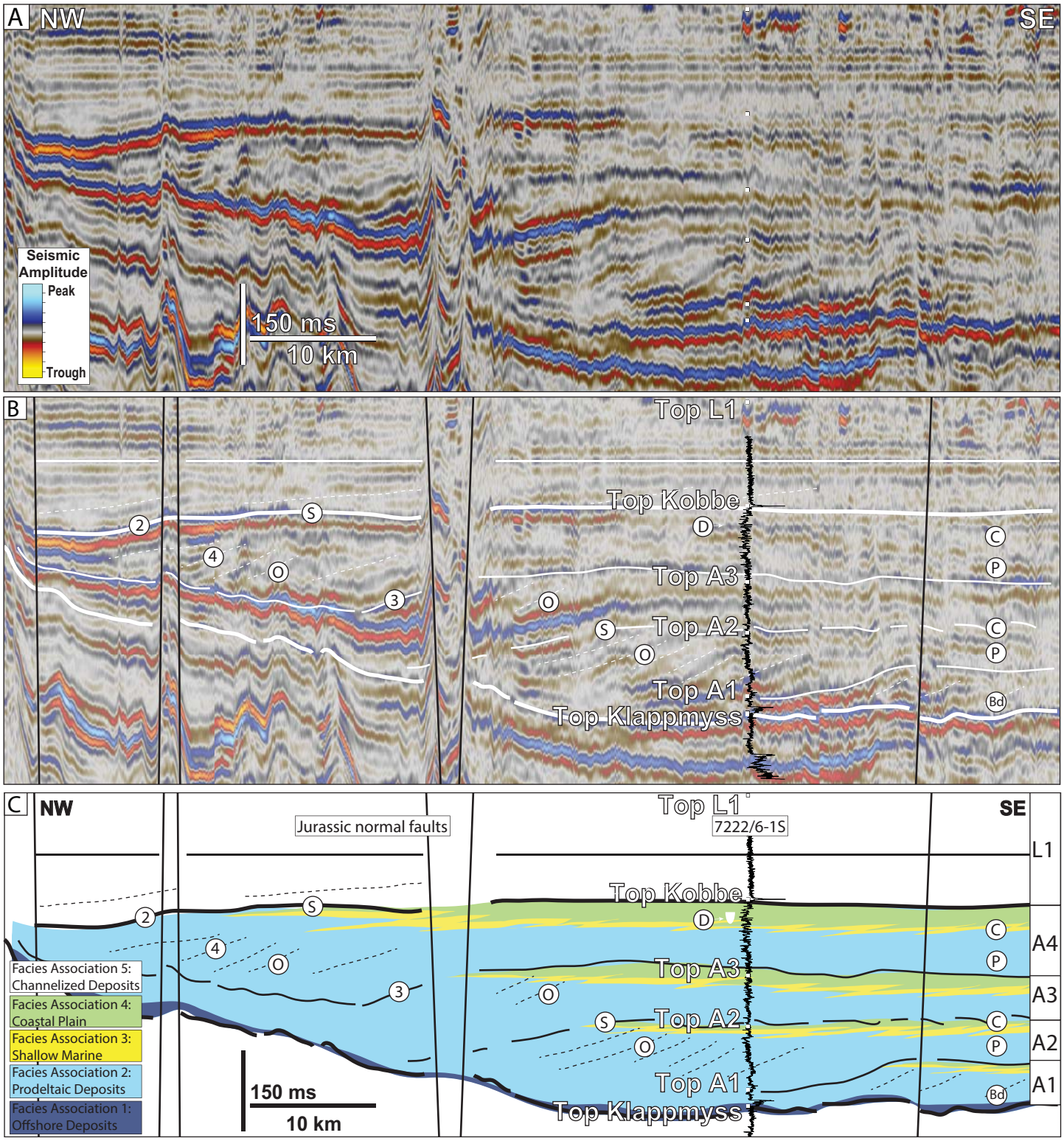

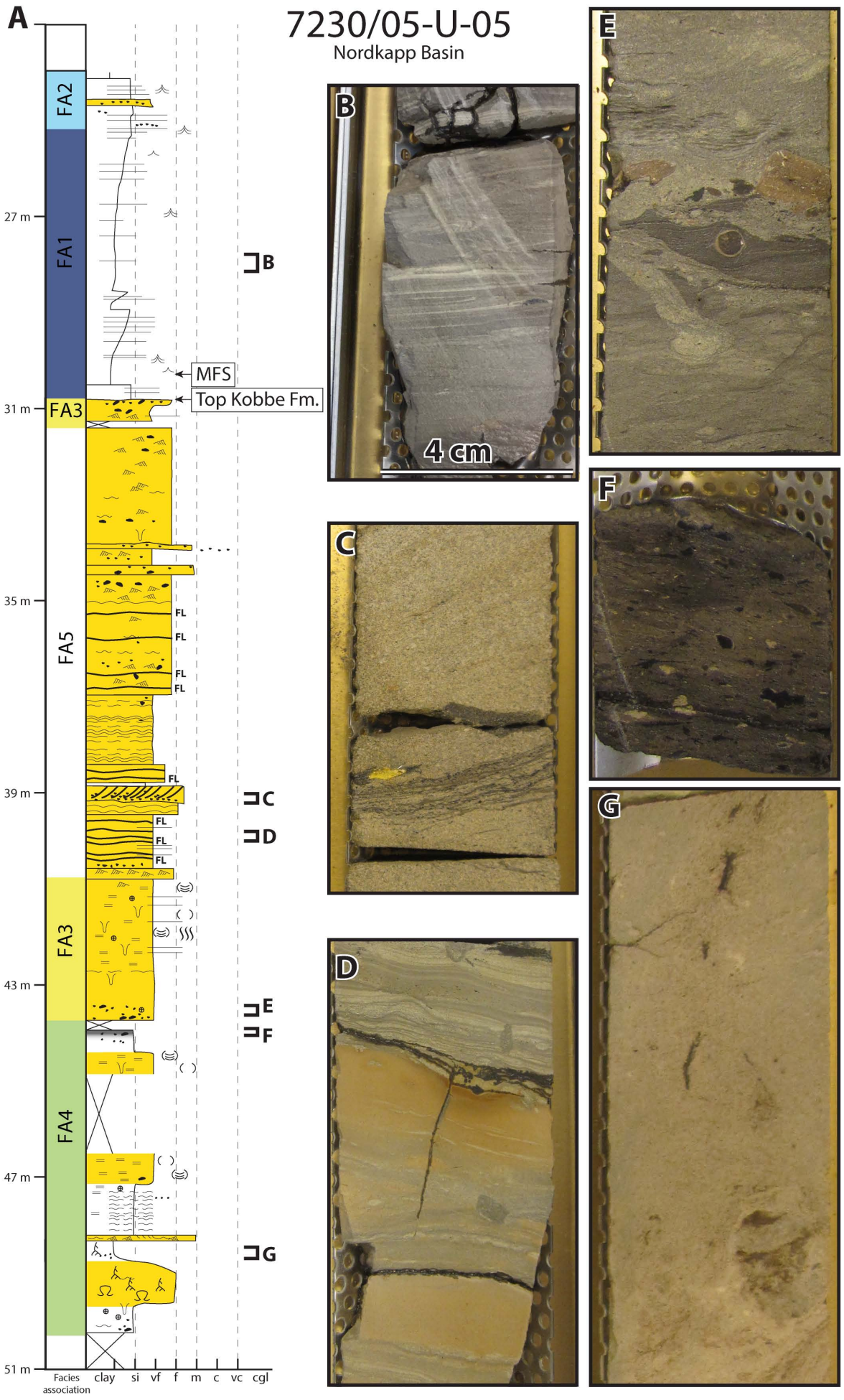

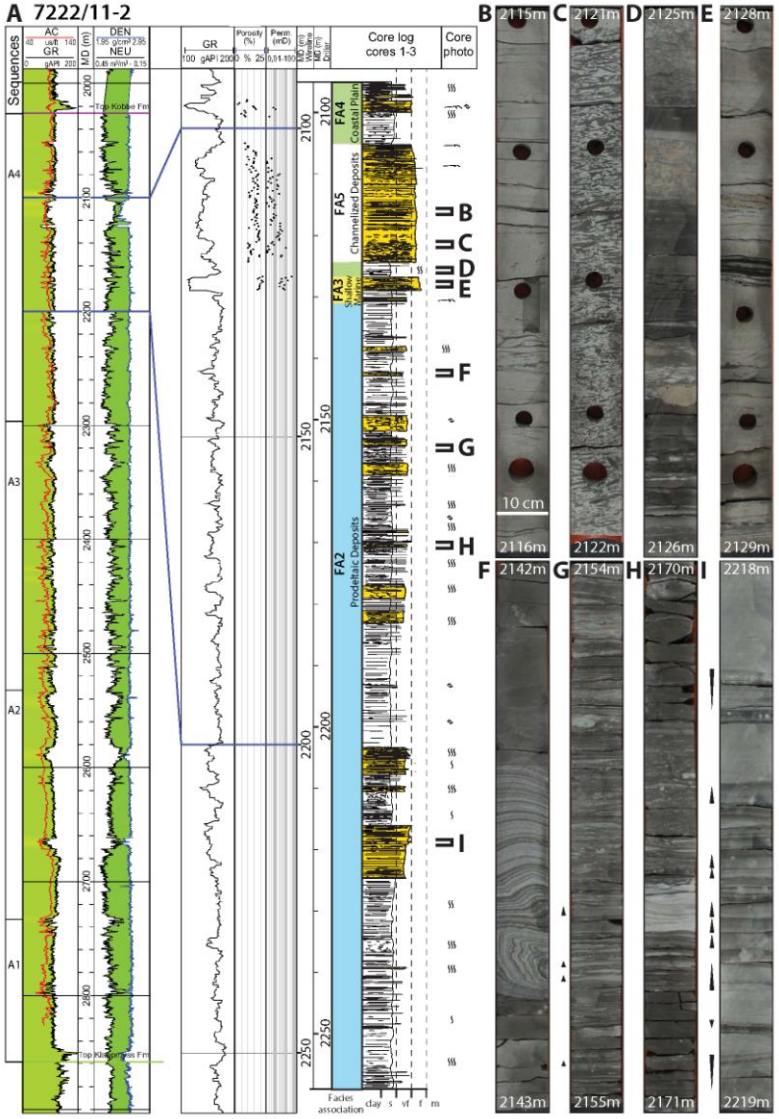

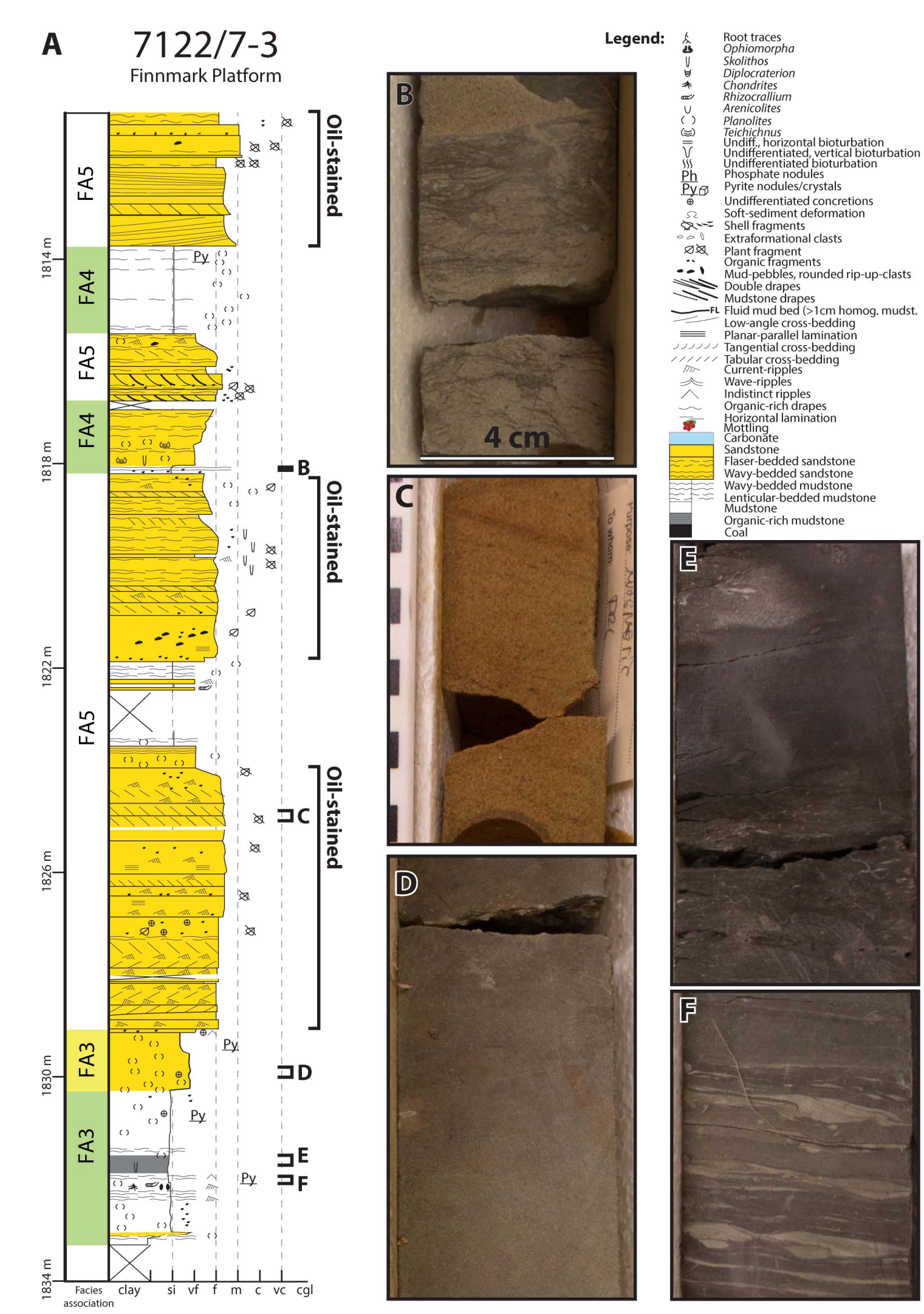
A
7122/7-3
Finnmark Platform
FA5
FA4
FA5
FA4
FA5
FA3
FA3
1814 m
1818 m
1822 m
1826 m
1830 m
1834 m
Py
Py
Py
Py
B
C
D
E
F
Oil-stained
Oil-stained
Oil-stained
Facies association
clay
si
vf
f
m
c
vc
cgl
B
4 cm
C
D
E
F
Legend:
Root traces
Ophiomorpha
Skolithos
Diplocraterion
Chondrites
Rhizocrallium
Arenicolites
Planolites
Teichichnus
Undiff., horizontal bioturbation
Undifferentiated, vertical bioturbation
Undifferentiated bioturbation
Phosphate nodules
Pyrite nodules/crystals
Undifferentiated concretions
Soft-sediment deformation
Shell fragments
Extraformational clasts
Plant fragment
Organic fragments
Mud-pebbles, rounded rip-up-clasts
Double drapes
Mudstone drapes
FL Fluid mud bed (>1cm homog. mudst.
Low-angle cross-bedding
Planar-parallel lamination
Tangential cross-bedding
Tabular cross-bedding
Current-ripples
Wave-ripples
Indistinct ripples
Organic-rich drapes
Horizontal lamination
Mottling
Carbonate
Sandstone
Flaser-bedded sandstone
Wavy-bedded sandstone
Wavy-bedded mudstone
Lenticular-bedded mudstone
Mudstone
Organic-rich mudstone
Coal